AD-A100 154   AERONAUTICAL RESEARCH ASSOCIATES OF PRINCETON INC NJ   F/G 19/1
APPLICATION OF THE INTEGRAL IMPACT THEORY TO MODELING LONG-ROD --ETC(U)
MAR 78 C V SWANSON, C D DONALDSON   DAAD05-76-C-0757
UNCLASSIFIED   ARAP-333   NL

1 OF 1
AD
A100154

END
DATE
FILMED
7-81
DTIC

LEVEL II

(2)

AD A100154

APPLICATION OF THE INTEGRAL IMPACT THEORY TO MODELING LONG ROD PENETRATORS

AERONAUTICAL RESEARCH ASSOCIATES OF PRINCETON, INC.
50 WASHINGTON ROAD, P.O. BOX 2229
PRINCETON, NEW JERSEY 08540

MARCH 1978
INTERIM REPORT FOR PERIOD 15 DECEMBER 1976 - 15 NOVEMBER 1977

PREPARED FOR

BALLISTIC RESEARCH LABORATORIES
ABERDEEN PROVING GROUND, MARYLAND 21005

THE VIEW, OPINIONS, AND/OR FINDINGS CONTAINED IN THIS REPORT ARE THOSE OF THE AUTHORS AND SHOULD NOT BE CONSTRUED AS AN OFFICIAL DEPARTMENT OF THE ARMY POSITION, POLICY OR DECISION, UNLESS SO DESIGNATED BY OTHER DOCUMENTATION.

UNCLASSIFIED

SECURITY CLASSIFICATION OF THIS PAGE (When Data Entered)

REPORT DOCUMENTATION PAGE		READ INSTRUCTIONS BEFORE COMPLETING FORM
1. REPORT NUMBER	2. GOVT ACCESSION NO. AD-A100154	3. RECIPIENT'S CATALOG NUMBER
4. TITLE (and Subtitle) APPLICATION OF THE INTEGRAL IMPACT THEORY TO MODELING LONG-ROD PENETRATORS		5. TYPE OF REPORT & PERIOD COVERED Interim 15 Dec '76 — 15 Nov '77
		6. PERFORMING ORG. REPORT NUMBER A.R.A.P. Report No. 333
7. AUTHOR(s) Claude V. Swanson, Coleman duP. Donaldson		8. CONTRACT OR GRANT NUMBER(s) DAAD05-76-C-0757
9. PERFORMING ORGANIZATION NAME AND ADDRESS Aeronautical Research Associates of Princeton, Inc., 50 Washington Road Princeton, New Jersey 08540		10. PROGRAM ELEMENT, PROJECT, TASK AREA & WORK UNIT NUMBERS
11. CONTROLLING OFFICE NAME AND ADDRESS Defense Advanced Research Projects Agency 1400 Wilson Boulevard Arlington, Virginia 22209		12. REPORT DATE March 1978
		13. NUMBER OF PAGES 79
14. MONITORING AGENCY NAME & ADDRESS (if different from Controlling Office) ARAP-333		15. SECURITY CLASS. (of this report) UNCLASSIFIED
		15a. DECLASSIFICATION/DOWNGRADING SCHEDULE

16. DISTRIBUTION STATEMENT (of this Report)

Approved for public release, distribution unlimited.

17. DISTRIBUTION STATEMENT (of the abstract entered in Block 20, if different from Report)

18. SUPPLEMENTARY NOTES

19. KEY WORDS (Continue on reverse side if necessary and identify by block number)

Integral Theory of Impact
Impact
Armor
Penetrator
Material Properties

20. ABSTRACT (Continue on reverse side if necessary and identify by block number)

The A.R.A.P. Integral Theory of Impact is applied to the problem of modeling long-rod penetrator performance. The rod penetrator is approximated by two cells, one which models the deforming hydrodynamic and plastic region at the leading edge of the rod, and a second cell which models the non-deforming portion of the shaft. Equations of motion are derived based on global conservation of momentum and energy. The material

DD FORM 1473, 1 JAN 73 — EDITION OF 1 NOV 65 IS OBSOLETE

UNCLASSIFIED

SECURITY CLASSIFICATION OF THIS PAGE (When Data Entered)

TABLE OF CONTENTS

I. INTRODUCTION

The purpose of this report is to document the significant results of the second year of our research program under Contract No. DAAD05-76-C-0757. The object of this portion of the program was to apply the A.R.A.P. Integral Theory of Impact to the problem of modeling the behavior of long rod penetrators.

Over the past several years the Integral Theory of Impact has been developed by A.R.A.P.[1-5] It is already proving to be a useful tool in the design of armor and penetrators. The theory contains the essential physics of the impact process, satisfies all the global conservation equations and is contained in a computer code which is simple and inexpensive to operate. The integral theory requires far less empirical information than some models and avoids the high cost and complexity of multi-element codes. Its simplicity introduces a degree of economy that makes it reasonable to conduct parametric studies so that predicted trends are available, rather than single point predictions. This aspect of the simple theory greatly facilitates the interpretation of observations and the selection of effective designs. The integral theory can, therefore, be used to guide experimental programs and to select those designs which warrant further study using the large codes.

The Integral Theory of Impact assumes that the energy of an incoming projectile is absorbed by the armor in one of three forms:

1.) As dissipated energy in the form of plastic work as the target flows around the penetrator, or as fracture energy in newly created fracture surfaces. This nonrecoverable portion of the total energy is characterized by an energy per unit mass of target material, E_{*p} , and it appears to be roughly independent of velocity for each material. The product of target density times E_{*p} corresponds to the "adiabatic hardness" of the material, or its hardness measured at the strain rates of impact.

2.) As elastic energy absorbed by the target in its local elastic deformation near the penetrator and in large scale elastic deformation modes. This elastic, or recoverable, portion of the total energy is parameterized by E_{*e} , the elastic energy per unit target mass. E_{*e} is a well defined function of p/d so a single constant defines E_{*e} for each material over the complete velocity range.

3.) As kinetic energy in the target material as it accelerates and begins to flow around the incoming penetrator. This portion of the energy is expressed by $\frac{C_D}{2} V^2$, where V is the velocity of the penetrator face relative to the target and C_D is a drag coefficient approximately equal to 1.0 for a penetrator with a spherical front end.

Similarly, when analyzing the dynamics of the deforming penetrator itself, there will be a quantity which measures the dissipated energy per unit mass absorbed by the penetrator as it deforms plastically or fractures. It is the analogue of E_{*p} for the target material. We will call this quantity E_{*d} . For ductile materials, the product of penetrator density times E_{*d} corresponds to the "adiabatic yield strength" of the material, which is the uniaxial yield strength of the material measured at the strain rates of impact. E_{*d} is assumed to be a constant for each penetrator material.

The kinetic energy in a deforming penetrator is modeled assuming a simple, usually linear, flowfield in the penetrator, and simple shapes such as cubes or cylinders to approximate the deformed shape of the projectile. The elastic energy in penetrators, analogous to E_{*e} for targets, has been neglected so far because it is relatively small compared to E_{*d} at the velocities of impact. However, in principle it can be included also.

Once the two parameters E_{*p} and E_{*e} are known for a target material, and E_{*d} is known for the penetrator, the behavior of the armor and penetrator during impact can be

computed from global energy and momentum conservation laws by the A.R.A.P. Integral Theory. Since it is only the sum of E_{*p} and E_{*e} which governs target performance, we shall often refer to the sum as E_* . E_{*p} and E_{*e} have been measured in impact tests for a variety of target materials from lead to boron carbide, from salt to Rolled Homogeneous Armor, over a velocity range from 20 ft/sec to 6,400 ft/sec and have been shown to provide an excellent description of armor behavior.[4] Although E_* for a target is measured in impact tests with nondeforming tungsten carbide balls, the same value of E_* for the target correctly predict its performance when the impactor is highly deforming, such as lead or soft aluminum spheres,[5] or with a high L/D, such as a long rod penetrator.

Recently, a theory has been developed which related E_{*p} and E_{*e} to more fundamental materials properties, such as melting temperature, heat capacity, Young's modulus and Brinell hardness.[4] This makes possible the prediction of armor performance from static tests alone. The theory has been verified experimentally over the same wide range of materials for which impact experiments have been conducted. It accurately predicts E_* to about ±15 percent for all these materials. This formula has enabled A.R.A.P. to conduct parametric studies, using handbook properties of materials, which have pointed up many promising lightweight armor materials, including some which are remarkably economical.

In this paper, we shall report that E_{*d} for penetrators can also be computed from the same fundamental materials properties, and can therefore be predicted from purely static tests. Thus, all the input parameters required to predict penetration by a deforming penetrator into a target can be obtained from handbook values of materials properties.

II. INTEGRAL THEORY FOR ROD PENETRATION

The Rod Penetrator Code to be described here, which we refer to as "ROD," uses the Integral Theory approach outlined in the introduction. As a penetrator moves through a target material with some velocity V_{face} at the penetrators front face, the Integral Theory for target performance tells us that the pressure at this face must be

$$\text{Pressure} = \rho_t \left(\frac{C_D}{2} V_{face}^2 + E_{*t} \right) \quad , \tag{1}$$

where ρ_t is the target density and $\rho_t E_{*t}$ the adiabatic hardness of the target material. $C_D \doteq 1$ for a nondeforming spherical front face, as reported previously. This formula has been verified for rigid sphere penetrators and deforming sphere penetrators over a wide range of projectile and target materials and velocities. Below we set up the equations governing the internal dynamics of a long rod penetrator which, when coupled with Eq. (1), which governs the target dynamics, completely specifies the problem.

It is known from X-ray photographs that the stages of long rod penetration may be roughly characterized as in Fig. 1. As the rod impacts the target the pressures generated at the interface begin to deform the front end of the penetrator, is in Fig. 1b. Simultaneously the target is eroded away by the same pressure, producing a crater, as in Fig. 1c. As penetration continues, material at the leading face of the penetrator is eroded away by the target, forced out laterally from the contact region by the high pressure there and ejected back out of the crater. As material is eroded from the rod face, new material is supplied to this region by the shaft of the rod, which is traveling at a higher velocity than the rod-target interface. At some point, Fig. 1d, the shaft material is used up and the head is decelerated quickly to zero velocity by the target.

We shall model the flowfield of a rod by dividing it into two regions; the head, corresponding to the front region of a

FLOW FIELD OF ROD AT VARIOUS STAGES OF PENETRATION

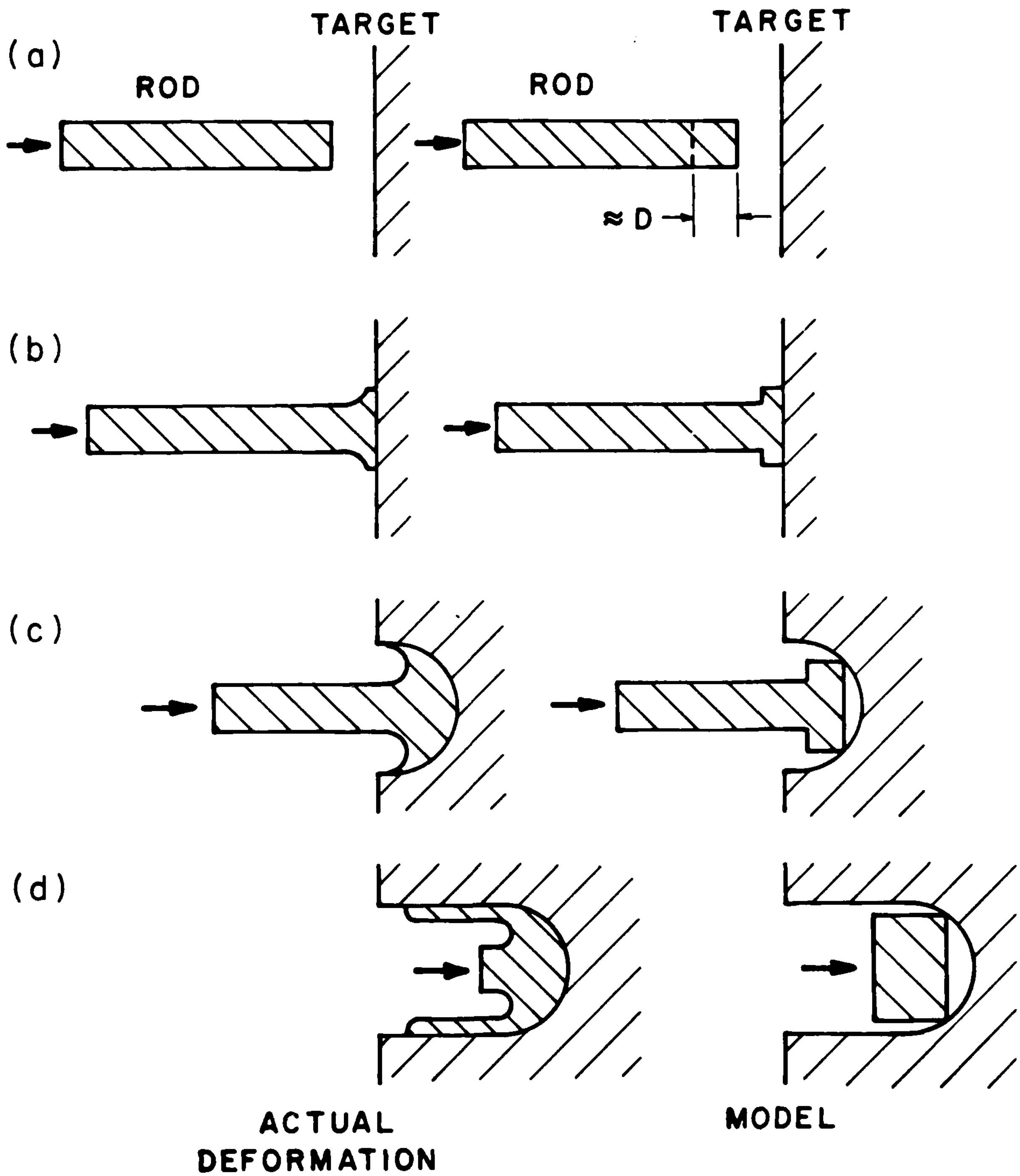

Figure 1

LONG ROD MODEL

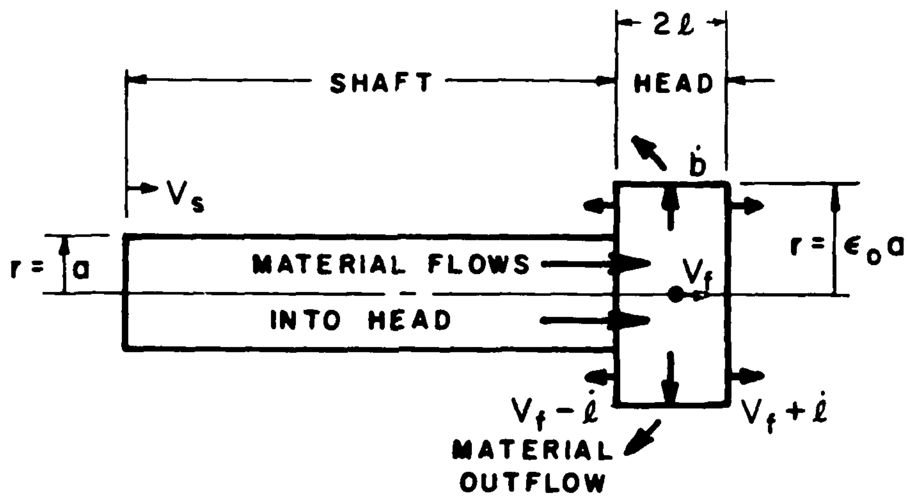

ASSUMPTIONS:

1. Conservation of energy
2. Conservation of momentum
3. Linear flow field in head
4. Continuity of mass flow across interface
5. Constant yield stress at interface
6. Mass of penetrator erodes from head when radius exceeds $\epsilon_0 a$
7. The model depends upon two parameters:

   The yield stress $Y_0 \cong \rho E_{*d}$

   and

   The shearing radius given by $\epsilon_0 a$

Figure 2

rod which is undergoing plastic and hydrodynamic strain, and a rear portion of the rod, the shaft, which we assume to be undeformed rod material. In Fig. 2, the assumptions and parameters of the model are summarized. During penetration the head, which is in contact with the target, decelerates and spreads laterally. We assume the mass flowfield in the head is linear, and the head is of cylindrical shape. The motion of the material in the head is characterized by a center of mass velocity V_f, and by the velocity of its front face $\dot{\ell}$ and side face $\dot{b}$ relative to the center of mass of the head. Conservation of mass across the boundary between the shaft and the head imposes the condition that the rate of flow of material from the shaft into the head is

$$\dot{M}_a = \pi a^2 \rho_p (V_s - V_f + \dot{\ell}) \tag{2}$$

where a is the radius of the shaft, ρ_p the penetrator density, and V_s the velocity of the shaft.

As penetration proceeds, the head widens as rod material is forced to flow in the lateral direction. At some distance from the axis of the rod, say $\varepsilon_o a$, we assume the flow of rod material has been turned or sheared off by the target and no longer can apply decelerating forces to the rod. Thus, when rod material in the head moves beyond a distance $\varepsilon_o a$, laterally, it is assumed to be detached from the rod. The dynamics of that material as it is further slowed by the target will not affect the deceleration of the shaft or head. This assumption is justified for some $\varepsilon_o a$ because the rod material at this point in the flow has been adiabatically heated so much by plastic work that its shear strength is very low, so it is only able to influence the rod through compressive or hydrodynamic forces. However, the axial force component of the compressive hydrodynamic force on the rod shaft will only be significant within one or two rod radii from the central axis. Thus, we shall expect $\varepsilon_o a \lesssim 2a$. Thus, $\varepsilon_o a$ really characterizes the turning radius

of the rod material in the target or the shape of the flowfield in the head. We further assume for simplicity that the shape of the flowfield in the head region of the rod does not change too much from material to material. Therefore, we may take ε_o to be the same constant for all rod penetrators, no matter what material.

When b (the radius of the rod head) reaches $\varepsilon_o a$, the cut-off radius, we assume any further increase in the radius of the head simply results in loss of rod material across the boundary at $\varepsilon_o a$, as in Fig. 2. The rate of mass loss from the head will be

$$\dot{M}_b = 4\pi \ell b \rho_p \dot{b} \tag{3}$$

where $\dot{b}$ is the lateral velocity of material in the head of the radius b. Then the rate of change of mass in the head is

$$\frac{d}{dt} M_f = \dot{M}_a - \dot{M}_b \tag{4}$$

and the rate of change of mass in the shaft is

$$\frac{d}{dt} M_s = - \dot{M}_a \tag{5}$$

The pressure applied to the rod front face by the target during penetration is

$$\rho_t (E_* t + \frac{C_D}{2} (V_f + \dot{\ell})^2) \tag{6}$$

as described in Eq. (1), where the front face of the rod moves at the velocity $V_f + \dot{\ell}$. This pressure acts across the entire frontal area of the rod head which is in contact with the target. The area is πb^2 giving

$$\text{Total force} = \frac{d}{dt} (M_f V_f + M_s V_s) = -\pi b^2 \rho_t (E_* t + \frac{C_D}{2} (V_f + \dot{\ell})^2) - \dot{M}_b V_f \tag{7}$$

from total conservation of momentum. The second term on the right accounts for momentum loss through mass loss out the side of the head. Substituting from (4), we find

$$\dot{M}_a (V_f - V_s) + M_f \dot{V}_f + M_s \dot{V}_s = -\pi b^2 \rho_t \left((E_* t + \frac{C_D}{2} (V_f + \dot{\ell})^2 \right) \tag{8}$$

This may be separated into two equations for the conservation of momentum of the head and the shaft. The shaft will only experience decelerating forces if it has a nonzero yield strength σ. In this case, we have

$$(\text{Force on Shaft}) = -\pi a^2 \sigma = M_s \dot{V}_s \quad . \tag{9}$$

When $\sigma = 0$, as in the case of a shaped charge jet, which is liquid, the shaft velocity remains constant throughout penetration. Subtracting this from (8) above, the corresponding equation for the head is obtained:

$$M_f \dot{V}_f = -\pi b^2 \rho_t (E_{*t} + \frac{C_D}{2}(V_f+\dot{\ell})^2) + \sigma \pi a^2 + \dot{M}_a (V_s - V_f) \tag{10}$$

The first term on the right is the force on the head due to the target pressure, the second term is the acceleration of the head due to the push from behind applied by the yield strength of the shaft, and the third term is the momentum added to the head from the material passing into the head from the shaft.

The equations above account for momentum conservation. Next, we require energy conservation. The total kinetic energy in the rod is given by

$$K = M_s \frac{V_s^2}{2} + \frac{M_f V_f^2}{2} + \frac{M_f}{2\alpha} (\dot{\ell}^2 + \frac{3}{2} b^2) \tag{11}$$

where the third term on the right accounts for the internal kinetic energy in the flowfield of the head. $\alpha = 3$ for a cylindrical head. The total work per unit time done on the rod by the target is

$$\dot{U} = \rho_t \pi b^2 (V_f+\dot{\ell})(E_{*t} + \frac{C_D}{2}(V_f+\dot{\ell})^2) \tag{12}$$

This work is converted into either heating of the rod of changing the kinetic energy of the rod. The heating rate is given by the $\dot{W}$, the rate at which rod material is converted into the hydrodynamic state, given by

$$\dot{W} = \dot{M}_a \, E_{*d} \tag{13}$$

where E_{*d} is the "adiabatic yield strength" of the rod material, and $\dot{M}_a$ is the rate at which rod material enters the head. The conservation of total energy requires:

$$\dot{W} + \dot{K} + \dot{U} = 0 \tag{14}$$

Lastly, the parameter ℓ for the half-thickness of the head and b for the radius of the head are related to the mass of the head by

$$2\pi \ell b^2 \rho_p = M_f \tag{15}$$

These equations completely specify the problem. We solve them to obtain the following coupled set of differential equations.

$$\dot{M}_f = \dot{M}_a - \dot{M}_b \tag{16}$$

$$\dot{M}_a = \pi a^2 \rho_p (V_s - V_f + \dot{\ell}) \cdot f_1 \tag{17}$$

$$\dot{M}_b = 4\pi \ell b \rho_p \dot{b} \cdot f_2 \tag{18}$$

$$\dot{V}_f = -\frac{1}{M_f}\left(\pi b^2 \rho_t (E_{*t} + \frac{C_D}{2} (V_f+\dot{\ell})^2) + \dot{M}_a(V_f - V_s) - f_2 \cdot \sigma\pi a^2\right) \tag{19}$$

$$\dot{V}_s = -\sigma\pi a^2/M_s \tag{20}$$

$$\dot{K} = -(V_f+\dot{\ell})\pi b^2 \rho_t \left(\frac{C_D}{2} (V_f+\dot{\ell})^2 + E_{*t}\right) - \dot{M}_a \rho_p E_{*d} - \frac{\dot{M}_b}{2} (V_f^2 + \dot{b})^2 \tag{21}$$

$$\dot{b} = \frac{b}{2}\left(\frac{\dot{M}_a}{M_f} - \frac{\dot{\ell}}{\ell}\right) \tag{22}$$

$$\ddot{b} = K_4 + K_5 \ddot{\ell} \tag{23}$$

where

$$K_4 = (1 - f_2)\frac{\dot{b}^2}{b} + \left(\frac{\dot{\ell}}{\ell}\right)^2 \frac{b}{2} - \frac{b}{2}\left(\frac{\dot{M}_f}{M_f}\right)^2 - \frac{f_1 \pi a^2 \rho_p (\dot{V}_s - \dot{V}_f) + f_2 4\pi \ell b \rho_p \dot{b}\left(\frac{\dot{\ell}}{\ell}\right)}{2M_f} \tag{24}$$

and

$$K_5 = \frac{a^2 f_1}{4\ell b} - \frac{1}{2}\frac{b}{\ell} \tag{25}$$

$$\ddot{\ell} = \frac{\dot{K} + Q_2 - \frac{3}{2}\frac{M_f}{\alpha}\dot{b}K_4}{\frac{M_f}{\alpha}(\dot{\ell} + \frac{3}{2}\dot{b}K_5)} \tag{26}$$

where

$$Q_2 = -\left\{\dot{M}_f\left(\frac{\ell^2}{2\alpha} + \frac{\dot{b}^2}{\alpha} + \frac{V_f^2}{2}\right) - \frac{\dot{M}_a V_s^2}{2} + \frac{\dot{M}_b}{2}(\dot{b}^2 + V_f^2) + M_f V_f \dot{V}_f\right\} \tag{27}$$

and penetration rate

$$\dot{p} = V_f + \dot{\ell} \tag{28}$$

f_1 and f_2 are integer quantities introduced to allow the numerical integration to proceed smoothly at certain discontinuous transition points in the model.

f_1 remains 1 unless the mass M_s of the shaft becomes zero. This will happen when the shaft has been consumed by erosion. When the mass M_s becomes zero, $f_1 = 0$.

f_2 remains zero until b , the head radius, reaches $\varepsilon_o a$. Then f_2 becomes 1 , and prevents the radius of the head from increasing beyond $\varepsilon_o a$. Thus, mass loss at the head also begins to occur when $f_2 = 1$.

This set of equations is incorporated into the computer code ROD, which is reproduced in Appendix I. The input parameters required to operate the code consist only of the length and radius of the rod, the density of the rod material, and its adiabatic hardness ρE_* , plus corresponding quantities for the target. The other parameters in the set of equations above are disposed of in the following way: We have learned that σ , the yield strength of the rod, is just its "adiabatic uniaxial flow stress" or

$$\sigma = \rho_p E_{*d} \tag{29}$$

The cut-off radius ε_o is assumed to be a constant, $\varepsilon_o = 1.36$, for all materials. Furthermore, the penetration depth in the rod program is not very sensitive to the initial assumed value of ℓ, so we always set $\ell = a$, initially, but this assumption is not critical. The only input parameters needed to operate the code are the physical dimensions, velocities, and densities of the target and penetrators, plus the E_* values of the materials. The value of the plastic component of E_* for any material can be derived from the formula[†]

$$E_* = 0.55 \quad C_p T_m \; \ell n \left(\frac{\sigma_F(T_i, \dot{\varepsilon})}{.08 \rho C_p T_M} + 1 \right) \qquad (30)$$

as derived in our previous interim report,[1] where C_p is the head capacity, T_m the melting temperature, ρ the density and σ_F the strain rate corrected flow stress of the material. Figure 3 displays the value of E_* predicted by this formula as a function of Brinell hardness for a number of materials of interest. When elastic effects can be neglected as they can be for most armor materials, we simply take E_{*t} of the target equal to E_* in Eq. (30).

As we shall show in this report, for penetrators, the corresponding E_{*d} may be found from

$$E_{*d} = \chi E_* \qquad (31)$$

where $\chi = 0.42$ for the code ROD and E_* for the rod is computed by substituting the melting temperature, heat capacity, density and flow stress values of the rod material into (30).

[†]The values of the constants in (30) have been modified slightly from those given in Reference 1, as a result of more extensive impact data.

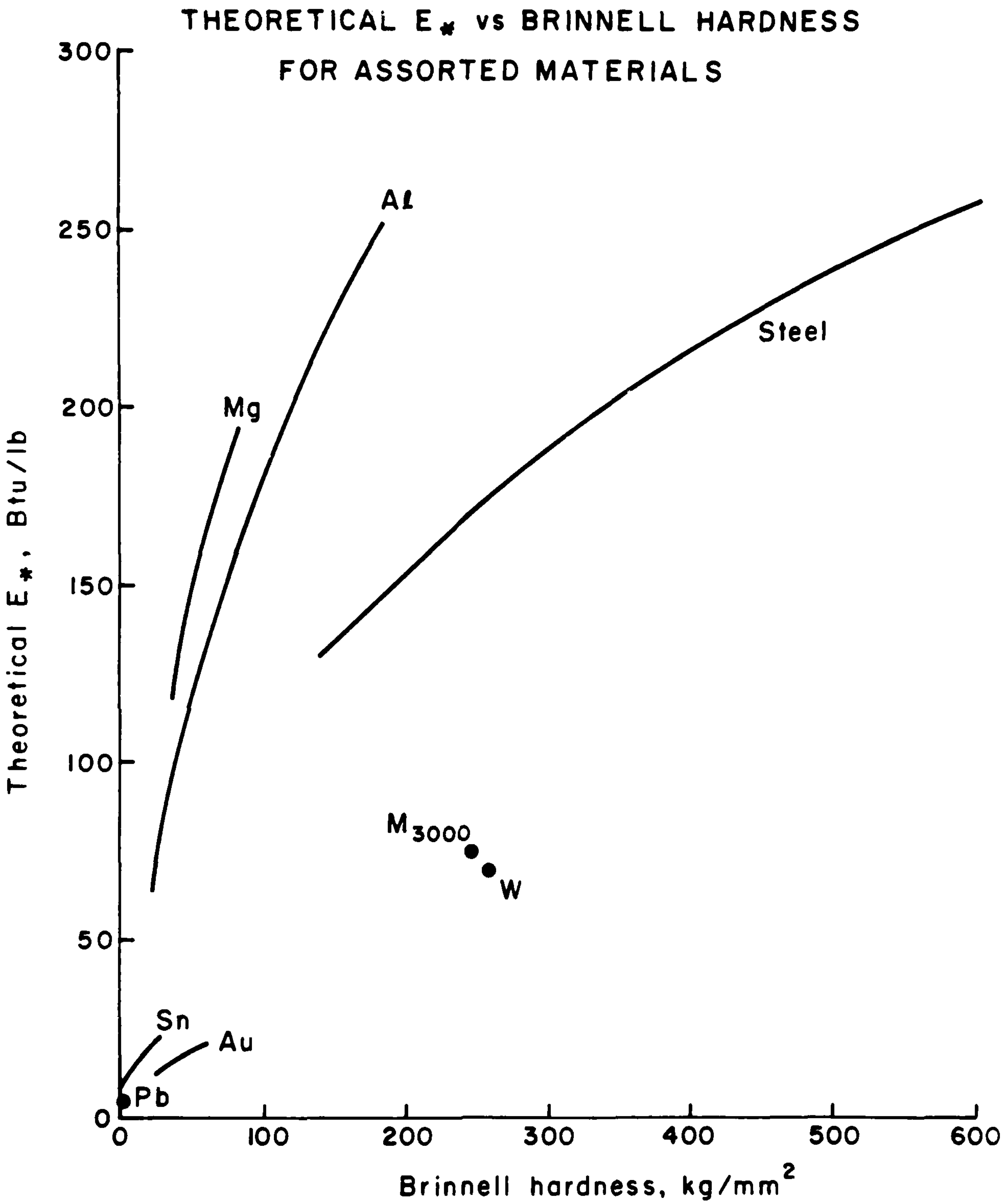
THEORETICAL E* vs BRINNELL HARDNESS
FOR ASSORTED MATERIALS
Theoretical E*, Btu/lb
Brinnell hardness, kg/mm²
0
50
100
150
200
250
300
0
100
200
300
400
500
600
Al
Mg
Steel
M3000
W
Sn
Au
Pb

Figure 3

III. DISCUSSION OF THE SIMPLIFIED CODE "PEN"

Recently a second model for rod penetration has been developed which is conceptually equivalent to the code ROD, but requires considerably less computer running time and is more useful for analytical investigations because of the simplicity of the equations. Most of the equations (16) - (28) are used in calculating the acceleration, energy and momentum in the flowfield of the head. These can be replaced by a term in the equation of momentum conservation (19) which accounts for accelerations in the head. The resulting model and code is named "PEN."

As in the ROD code, a two-element rod is assumed, consisting of a shaft and a head. The cutoff radius $\varepsilon_o a$ is retained, and again is assumed to have a constant value, independent of rod material. The initial length of the head region is assumed to be a, and the volume of the head is assumed to be constant as it flattens and widens upon impact. Thus,

$$M_f = \pi a^3 \rho_p \ . \tag{32}$$

The decelerating force acting on the head is the sum of the decelerating forces provided by the target plus the accelerating force on the head supplied by the yield strength of the shaft:

$$M_f \dot{V}_f = - \pi b^2 \rho_t (E_* t + \frac{C_D}{2} V_f^2) + \pi a^2 \rho_p (E_* d + (V_s - V_f)^2) \tag{33}$$

where the first term on the right is the force exerted on the head by the target and the second term is the force which the shaft exerts on the head. The term $\rho_p (V_s - V_f)^2$ accounts for the momentum gained by the head from material which has entered the head from the shaft. The front face velocity of the rod is assumed to be equal to the center of mass velocity of the head, V_f. Substituting Eq. (32) into Eq. (33) produces

$$\dot{V}_f = \frac{1}{a\rho_p} \left(-\rho_t \frac{b^2}{a^2} \left(E_* t + \frac{C_D}{2} V_f^2\right) + \rho_p \left((V_s - V_f)^2 + E_* d\right)\right) \tag{34}$$

The corresponding equation for the velocity of the shaft is Eq. (20), which we rewrite as

$$\dot{V}_s = - \frac{1}{M_s} \pi a^2 \sigma \tag{35}$$

where

$$\sigma = \rho_p E_* d .$$

The penetration p of the rod is given by

$$\dot{p} = V_f , \tag{36}$$

and the erosion of the rod length L is governed by

$$\dot{L} = V_f - V_s . \tag{37}$$

The radius of the head b during the early stages of penetration when it is widening, is computed in the following way:

If ℓ is the thickness of the head,

$$\pi b^2 \ell \rho_p = M_f = \rho_p \pi a^3$$

yielding

$$\ell = \frac{a^3}{b^2} .$$

But since the initial thickness of the head is a, then $\ell = a - (L_o - L)$, for $b < \varepsilon_o a$, so

$$b = \begin{cases} \dfrac{a}{\sqrt{1 - \left(\dfrac{L_o - L}{a}\right)}} , & \dfrac{L_o - L}{a} \leq 1 - \dfrac{1}{\varepsilon_o^2} \\ \varepsilon_o a , & \dfrac{L_o - L}{a} > 1 - \dfrac{1}{\varepsilon_o^2} \end{cases} \tag{38}$$

defines b and completes the system of equations. This system of equations, Eq. (34) - Eq. (38), defines the numerical code PEN. As with the ROD code, the only input parameters required are the initial velocity of the rod, the values of E_* for the rod and target, and the dimensions and densities of the materials.

This model can be related to hydrodynamic models of rod penetrators in the following way. During steady-state penetration of a rod, V_f typically approaches some constant value $\sim \frac{1}{3} V_s$ - $\frac{1}{2} V_s$. During this stage of penetration, $\dot{V}_f$ may be neglected in Eq. (33). Assuming b has reached its full value of $\varepsilon_o a$, Eq. (34) may be approximated as

$$\rho_p (V_s - V_f)^2 = \rho_t \varepsilon_o^2 \frac{C_D}{2} V_f^2 + (\rho_t \varepsilon_o^2 E_* t - \rho_p E_* d) \qquad (39)$$

This equation may be compared to various models for rod penetration, such as that found in Ref. 6,7

$$\frac{1}{2} \rho_p (V_s - V_f)^2 = \frac{1}{2} \rho_t V_f^2 + (R - Y) , \qquad (40)$$

where R is the target strength and Y the strength of the penetrator. Dividing Eq. (39) by 2 and comparing coefficients, we find

$$\begin{aligned} \frac{1}{2} \varepsilon_o^2 C_D &\longleftrightarrow 1 \\ \frac{\rho_t \varepsilon_o^2 E_* t}{2} &\longleftrightarrow R \\ \frac{\rho_p E_* d}{2} &\longleftrightarrow Y \end{aligned} \qquad (41)$$

Now the values of R and Y which give the best fit to experiment for a number of materials have been deduced in Refs. (6-8). In Table 1, we compile the experimental values[6-8] of R and Y as well as our theoretical prediction of them based on Eq. (41) and the theoretical value for E_*, Eq. (30). The good agreement

TABLE 1

Material	ρ (kg/m^3)	E_* (BTU/1b)	$Y^{THEOR.}$ (MPa) ($\rho_p E_*/2$)	$Y^{EXP.}$ (MPa)	$R^{THEOR.}$ (MPa) ($\rho_p E_* \varepsilon_o^2/2$)	$R^{EXP.}$ (MP$_a$)
Cu	3920	38	398	380	1150	
1090 Steel	7800	130	1195	1200	3453	
Ta	16900	61	1216	900	3514	
Be	1881	407	888	350	2566	
U	18900	61	1337	1100	3866	
Mg(AZ80F)	1800	169	353	340	1020	
Al(6061)	2700	160	501	420	1031	
St 37 (B=135)	7800	135	1222		3531	3450
St 52 (B=180)	7800	145	1312		3791	4400
HzB20 (B=300)	7800	192	1737		5019	5175
St (B=230)	7800	160	1448	1100	4184	
D17 (B=270)	17000	80	1577	1550	4557	
Al(7075-T6)	2700	250	783		2262	2100

indicated by Table 1 strongly indicates that the parameters R and Y employed in the hydrodynamic models are related to the single fundamental material property E_* by Eq. (41).

Conceptually, then, the rod program PEN is equivalent to a hydrodynamic model with strength in the target and rod, such as Eq. (40), plus an additional term proportional to the deceleration of the rod front face, which takes into account inertial effects at the front of the rod during the early stages of impact before equilibrium of pressures has been established. This inertial term $M_f\dot{V}_f$ acts as an effective stiffening or strengthening of the rod during this early phase of penetration, and accounts for the observed fact that rods of lower L/D have a greater penetration vs. rod length, P/L , than large L/D rods do. Were it not for this term, and an additional small effect due to the initial spreading of front face, rods of all L/D would have the same penetration vs. length at the same velocity, as the hydrodynamic theory of Eq. (40) predicts.

The program PEN has been extremely useful as a means of gaining an intuitive understanding of rod penetration, since it can predict rod performance over the same range of materials and velocities as the ROD code, yet has simpler equations which can be dealt with and understood algebraically.

In Section VI, the predictions of PEN are compared to the code ROD and to experimental data for a wide range of materials and velocities. We have found that the value of ε_o and χ which gives the best fit to experiment for PEN is $\varepsilon_o = 1.7$, $\chi = 1.0$, and $C_D = 0.5$. These values are used in all computations employing the PEN code.

The relationship between the material strengths Y and R of Table 1 is reminiscent of the relationship between the uniaxial tensile strength and the Brinell hardness of a material in static tests. It is well known that the Brinell hardness B for a ductile material, which is just the pressure that a ductile target can sustain when impressed by a rigid ball indenter, may be related to the uniaxial flow stress of a rod of the same material by

$$\sigma \doteq (0.3)B \quad .$$

Similarly, the effective strength R of the target, which is analogous to B , may be related to the uniaxial strength Y of the rod, which is analogous to σ , by

$$\frac{Y^{THEOR.}}{R^{THEOR.}} = \frac{\rho_p E_*/2}{\rho_p E_* \varepsilon_o^2/2}$$

$$\longrightarrow Y^{THEOR.} = .34 \ R^{THEOR.}$$

This strongly suggests that the relationship between Y and R is just that between a uniaxial tensile test and a Brinell hardness test <u>done at the strain rates of impact</u>. Thus ρE_* , which determines both R and Y , is a true measure of a materials' strength at impact strain rates. The shear heating process in the deforming material at these strain rates is adiabatic rather than isothermal, since heat is generated locally in regions of shear much faster than it can dissipate by thermal conduction. When the local heating, with the attendant local softening of the material, is considered, as we discussed in Reference 4, Eq. (30) is derived for the effective material strength at impact strain rates. We refer to ρE_* as the "adiabatic hardness" of a material, and note that it determines both target and rod strengths at these strain rates.

The quasi-hydrodynamic model of Eq. (39) is useful in another way as a tool for analyzing qualitatively different regimes of penetration. If the target is very hard (high E_{*t}) then the rod will not penetrate unless its velocity is sufficiently high to overcome the target strength with kinetic energy. The condition for the lower limit of velocity required for penetration is formed by setting $V_f = 0$ in (39) and solving for V_s :

$$(V_s)_o = \sqrt{\frac{\rho_t}{\rho_p} \varepsilon_o^2 E_{*t} - E_{*d}} \quad .$$

Penetration will not occur unless the initial rod velocity exceeds $(V_s)_o$, according to this model. In reality, some penetration does occur below this velocity but, as in Figs. 31, 32 and 33, there usually is a long straight section of the P/L vs velocity curve which, when extrapolated to zero penetration, intersects the velocity coordinate at a value given approximately by $(V_s)_o$. See Ref. 6 for a discussion of this relating to the data in Fig. 31. The discrepancy at velocities below $(V_s)_o$ occurs because we have neglected the $\dot{V}_f$ term in Eq. (39).

When the rod is very strong compared to the target, it may not erode at all, and then it behaves like a nondeforming rod. This limit, in which $V_f = V_s$, will occur when

$$(V_s)_o = \sqrt{\frac{\rho_p E_* d - \rho_t \varepsilon_o^2 E_* t}{\rho_t \varepsilon_o^2 \frac{C_D}{2}}} \quad .$$

If the quantity under the radical is >0 , there will exist a value $(V_s)_o$ for which penetration of the rod can occur without erosion. For any initial velocity below $(V_s)_o$ the rod behaves as a nondeforming projectile, and the A.R.A.P. integral theory for nondeforming projectiles is employed instead of the deforming rod equation. For velocities above $(V_s)_o$ the deforming rod model applies. Figure 35, discussed in Section VI, affords a striking example of the transition from nondeforming penetration to deforming rod penetration as the striking velocity is increased.

IV. BACKFACE EFFECTS

In order to apply the A.R.A.P. integral theory to targets of finite thickness, backface effects must be included. The E_* concept was originally developed for the flow of target material around a penetrator in a semi-infinite target. The shear work done on the target material in the flow volume defines E_{*t}, the E_* for the target. When the projectile has penetrated almost all the way through the target, to within one or two diameters of the backface, the target material can spall or simply bulge on the backside, rather than flowing around the penetrator hydrodynamically. Thus, each small volume of target material absorbs less energy than it would in the semi-infinite case. Thus, the effective E_* for the target decreases near the backface, and we call this the backface effect.

In order to characterize the backface effect empirically, static Brinell hardness tests were performed on 1100-F aluminum and lexan sheets unsupported at the back, using a .250" diameter WC ball at very shallow and very deep penetrations. At the deep penetrations, backface effects in the target sample affected the hardness measurement. In Fig. 4, the Brinell hardness of a 1/4" thick 1100-F aluminum plate is measured vs. penetration depth of the ball, and plotted as curve (a). The hardness is roughly constant with penetration until the ball is about .150" from the backface, at which point the hardness begins to decrease linearly with further penetration. When the front face of the ball reaches .475" of "penetration," so it has actually passed through the plate, the bulge on the back of the plate fractures and the measured hardness drops to zero. For comparison, the hardness vs. penetration depth for the same WC ball in a semi-infinite 1100-F aluminum plate is plotted as curve (b). The ratio of measured hardness in the .250" thick plate to the measured hardness in the semi-infinite plate is plotted on the same graph as a solid curve, (c). It is clear that as the ball approaches within a diameter or so of the backface, the hardness begins to decrease monotonically with penetration. We should expect that ρE_*, which

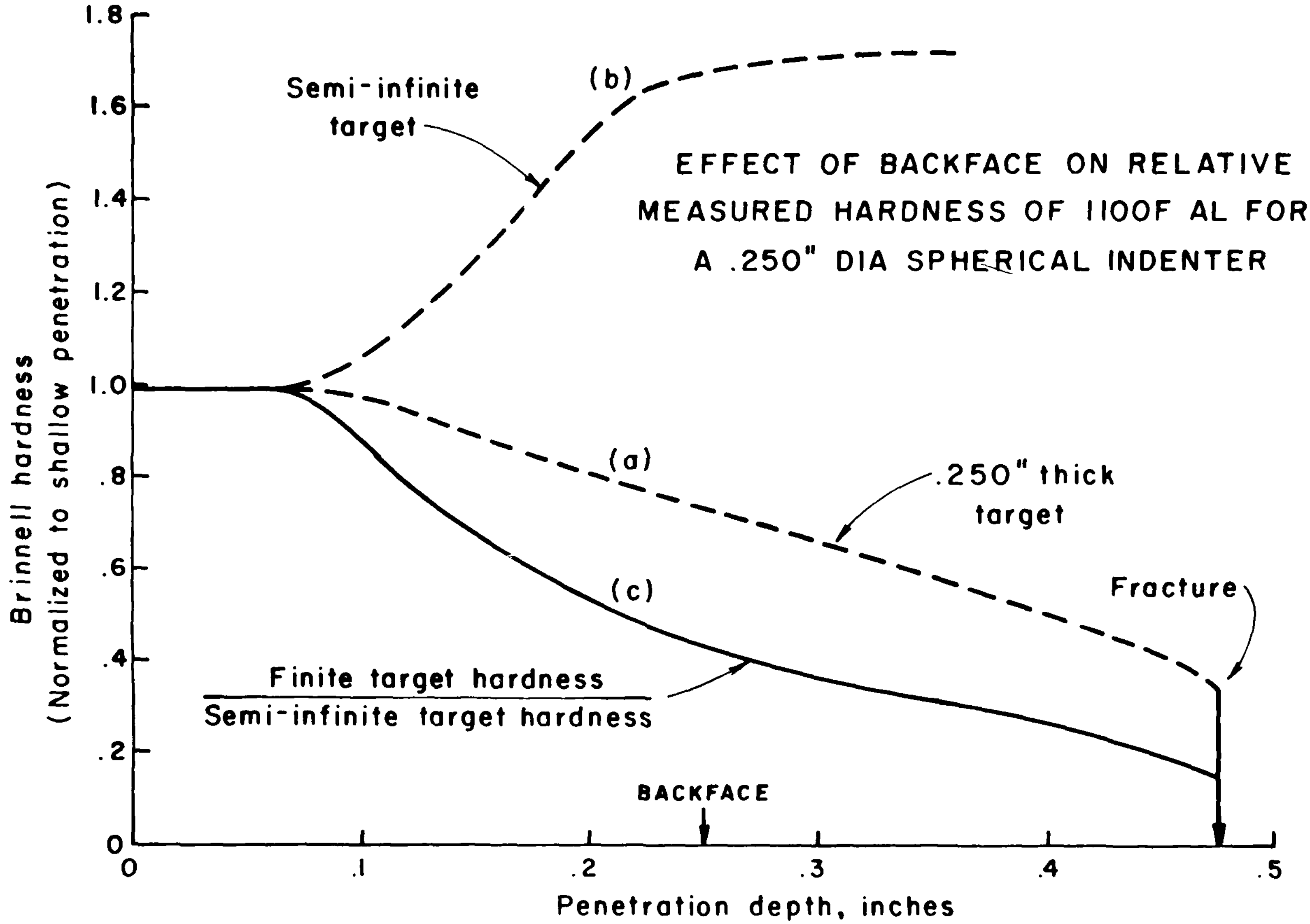
EFFECT OF BACKFACE ON RELATIVE
MEASURED HARDNESS OF 1100F AL FOR
A .250" DIA SPHERICAL INDENTER
Brinnell hardness
(Normalized to shallow penetration)
1.8
1.6
1.4
1.2
1.0
.8
.6
.4
.2
0
Semi-infinite
target
(b)
(a)
.250" thick
target
(c)
Fracture
Finite target hardness
Semi-infinite target hardness
BACKFACE
0
.1
.2
.3
.4
.5
Penetration depth, inches

Figure 4

measures the target strength at the strain rates of impact, should decrease in roughly the same way as the measured static hardness does near the backface.

In a second experiment, the Brinell hardness at deep penetration in lexan plates was measured over a range of plate thickness and ball diameters. The results are shown in Fig. 5. It was found that the results could be fit empirically by

$$\text{Brinell hardness } B = \begin{cases} Bo \ , & \tau - p \geq (\beta - 1)r \\ \dfrac{\tau - p + r}{\beta r} Bo \ , & \tau - p < (\beta - 1)r \end{cases} \tag{42}$$

where $\beta = 4$, B_o is the hardness of a semi-infinite lexan plate, τ is the plate thickness, p the penetration depth of the ball, and r the contact radius of the depression made by the ball in the target. Obviously, $r \leq a$, where a is the ball radius, and

$$r = \begin{cases} \sqrt{2ap - p^2} \ , & p \leq a \\ a \ , & p \geq a \end{cases} \tag{43}$$

In Fig. 6, this expression is compared with the measured value of relative hardness at various penetrations for the aluminum plate discussed in Fig. 4. The agreement is qualitatively good, although there are certainly other expressions which would characterize the hardness near the backface as well.

The form of expression, (Eq. (42), was chosen as our model for the backface because of the following intuitive model for backface effects. We assume that the flowfield of target materials around the penetrator extends for some distance in front of the penetrator. We expect this distance to be proportional to the contact radius r of the penetrator, and to extend a distance βr in front of the penetrator, from the point of maximum contact width. Thus, for a spherical indenter imbedded less then one radius deep in a target, the flowfield is assumed to extend a distance βr from the surface of the target. Once the ball is fully imbedded, then $r = a$, and the flowfield extends a distance βa in front of the ball, as measured from the center

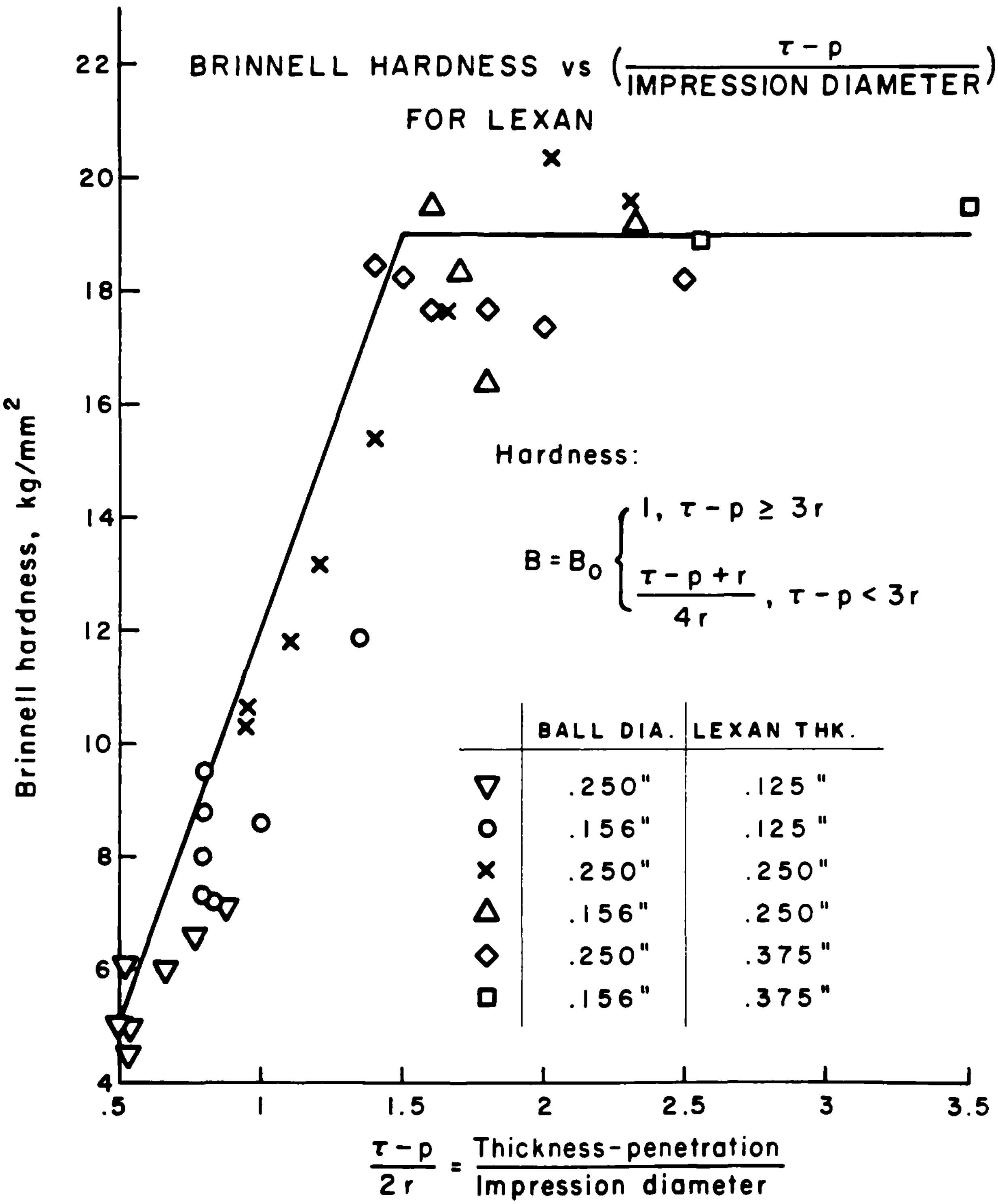

BRINNELL HARDNESS vs ($\frac{\tau - p}{\text{IMPRESSION DIAMETER}}$)
FOR LEXAN
Brinnell hardness, kg/mm^2
22
20
18
16
14
12
10
8
6
4
.5
1
1.5
2
2.5
3
3.5
Hardness:
$B = B_0 \begin{cases} 1, & \tau - p \geq 3r \\ \frac{\tau - p + r}{4r}, & \tau - p < 3r \end{cases}$
BALL DIA. | LEXAN THK.
▽ .250" .125"
○ .156" .125"
× .250" .250"
△ .156" .250"
◇ .250" .375"
□ .156" .375"
$\frac{\tau - p}{2r} = \frac{\text{Thickness-penetration}}{\text{Impression diameter}}$

Figure 5

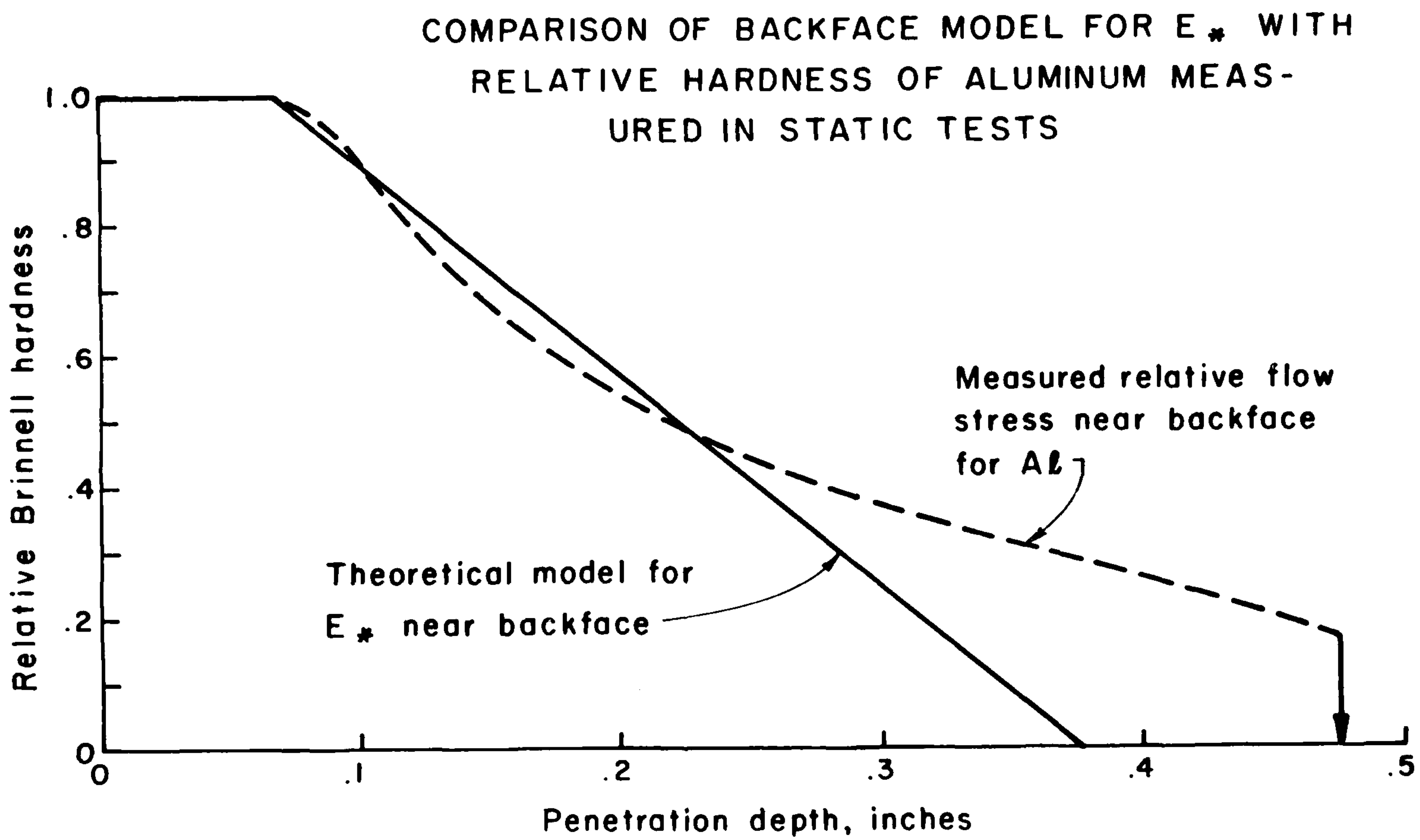

COMPARISON OF BACKFACE MODEL FOR E* WITH RELATIVE HARDNESS OF ALUMINUM MEASURED IN STATIC TESTS
Relative Brinnell hardness
1.0
.8
.6
.4
.2
0
0
.1
.2
.3
.4
.5
Penetration depth, inches
Measured relative flow stress near backface for Aℓ
Theoretical model for E* near backface

Figure 6

COMPARISON OF BACKFACE MODEL
WITH EXPERIMENT

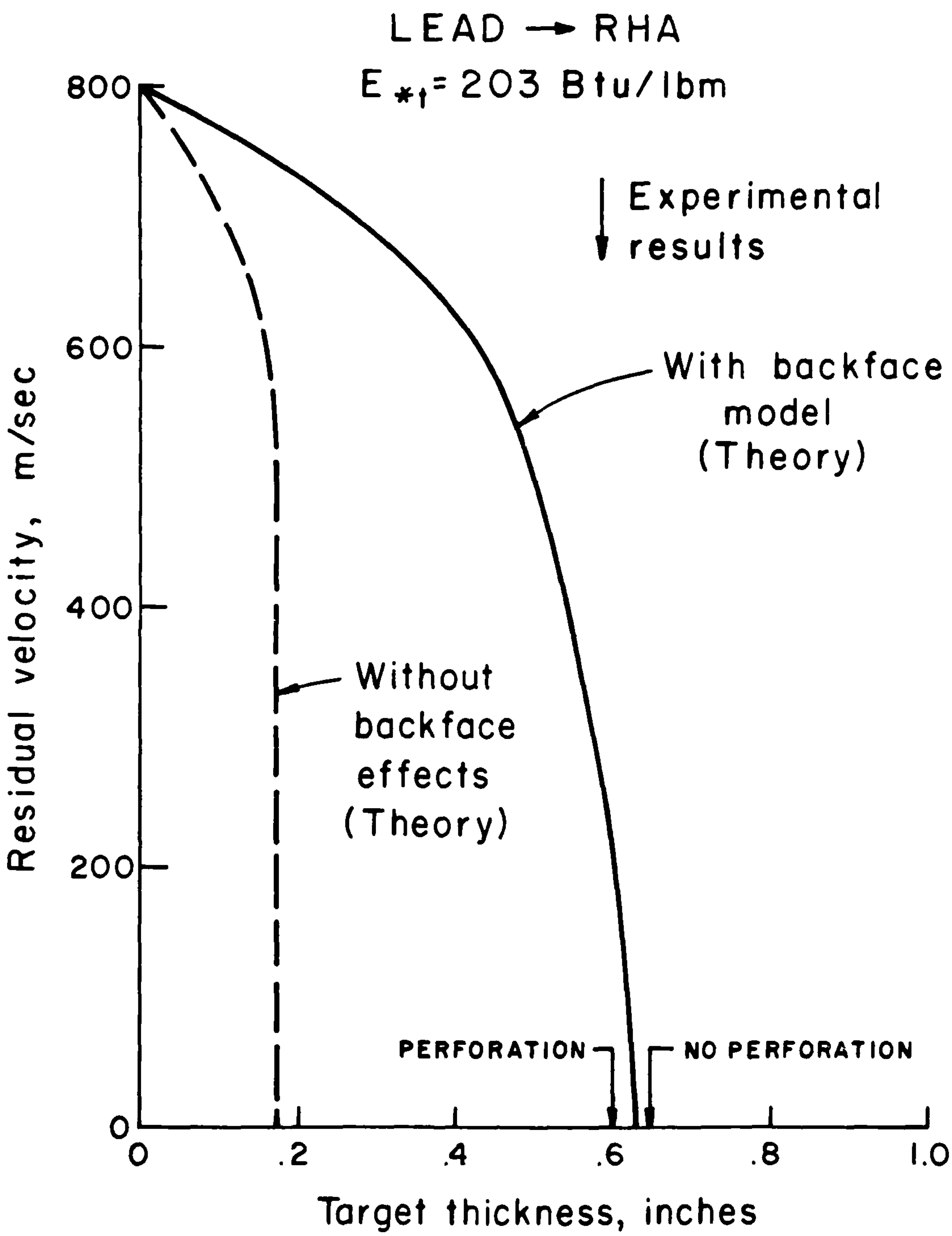

Figure 7

of gravity of the ball. Thus, the backface effect will begin to show up when $p - a = \tau - \beta a$ for a fully imbedded ball, hence Eq. (42). For a blunt nosed object, such as a cube or cylinder impacting end on into a target, the widest point of the penetrator occurs at the leading face, unlike the sphere. Then the backface effect begins to occur when

$$p = \tau - \beta a ,$$

so we can summarize:

<u>Backface Model</u>

For a sphere:

$$E_{*t} = \begin{cases} E_* & , \tau - p \geq (\beta - 1)r \\ E_* \left(\dfrac{\tau - p + r}{\beta r}\right) & , \tau - p < (\beta - 1)r \end{cases} \tag{44}$$

For a cube or cylinder:

$$E_{*t} = \begin{cases} E_* & , \tau - p \geq \beta r \\ E_* \left(\dfrac{\tau - p}{\beta r}\right) & , \tau - p < \beta r \end{cases} \tag{45}$$

We have made the assumption here that the dynamic stength of the target, E_* , decreases near the backface in the same way as the static strength does. We do not *a priori* expect these formulas with the same constants to work well for all materials, since brittle materials will show spall and other backface effects when the penetrator is many diameters from the backface. It is possible that by making β inversely proportional to the failure strain of the target, the formula may be generalized. Such approaches will be considered in subsequent work. For many ductile materials, however, we have found that Eq. (44) and Eq. (45) accurately describe the decrease of E_* near the backface.

As an example, refer to Figs. 7, 8 and 9 in which nondeforming tungsten carbide balls and highly deforming lead projectiles were fired into rolled homogeneous armor, 5083 aluminum,

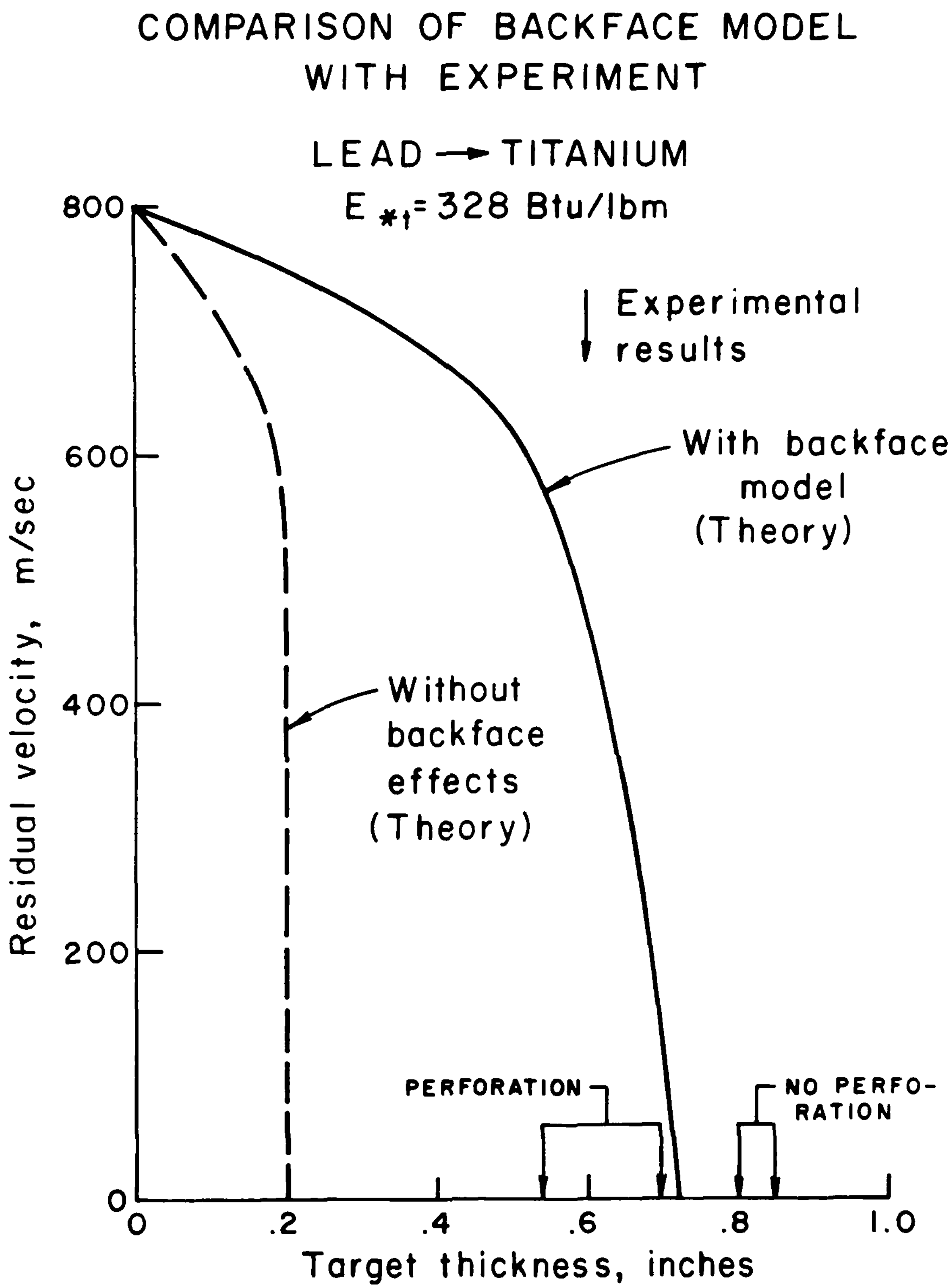
COMPARISON OF BACKFACE MODEL
WITH EXPERIMENT
LEAD → TITANIUM
E_{*t} = 328 Btu/lbm
Experimental
results
With backface
model
(Theory)
Without
backface
effects
(Theory)
PERFORATION
NO PERFO-
RATION
800
600
400
200
0
Residual velocity, m/sec
0
.2
.4
.6
.8
1.0
Target thickness, inches

Figure 8

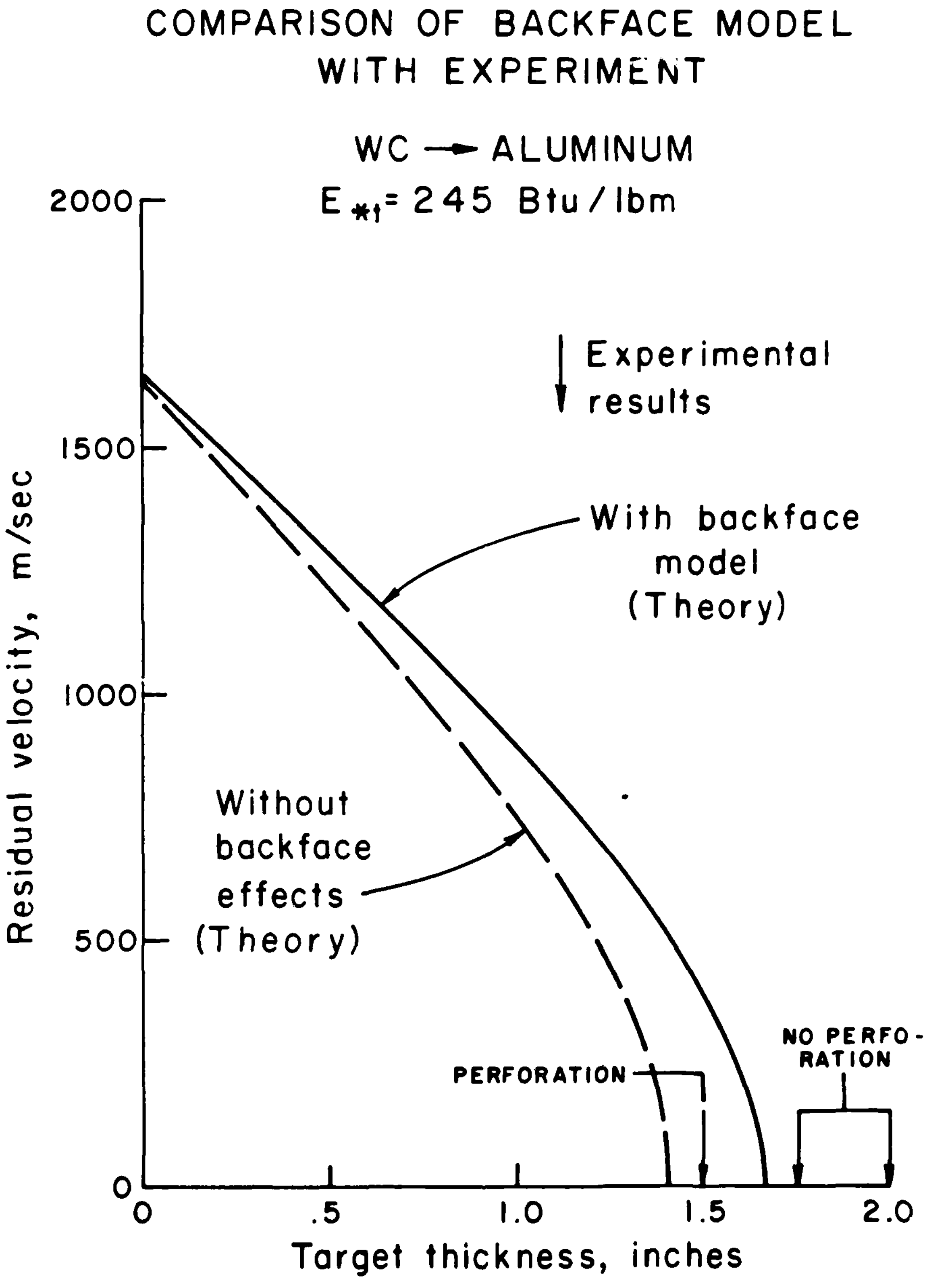
COMPARISON OF BACKFACE MODEL
WITH EXPERIMENT
WC → ALUMINUM
E_{*t} = 245 Btu/lbm
2000
1500
1000
500
0
Residual velocity, m/sec
Experimental
results
With backface
model
(Theory)
Without
backface
effects
(Theory)
PERFORATION
NO PERFO-
RATION
0
.5
1.0
1.5
2.0
Target thickness, inches

Figure 9

and titanium armor. In each case the theoretical residual velocity of the projectile is plotted vs. target thickness for a given initial projectile velocity, using the A.R.A.P. rigid sphere and deforming cube programs and the backface model of Eqs. (44) and (45). In all cases, $\beta = 4$. The theoretical values of E_* , which have been verified for each material in the semi-infinite case, were used in this calculation. In the same figure are plotted the predicted residual velocities for no backface effect. The value of target thickness at which the residual velocity equals zero measures the stopping thickness required for each projectile at the indicated initial velocity. Arrows on each figure indicate the experimental thickness which stopped or failed to stop the projectile. We conclude that the backface model with $\beta = 4$ works quite well for RHA, titanium and 5083 aluminum.

It should be pointed out that there are exceptions to this model. Certain composite materials, such as fiberglass and Kevlar woven rovings are better modeled as having no backface effects, or $\beta << 1$. Similarly, brittle materials act as though $\beta >> 4$. Fortunately, however, a large number of ductile materials including many important armor materials are described by $\beta = 4$.

V. OBLIQUE PENETRATION

When a rod impacts an armor plate at an oblique angle, the forces on the rod will not be axially symmetric. Thus we include in the rod program a lateral force F_L acting on the head of the rod, as well as the axial force F_A, which was described in Sections II and III. A bending mode, characterized by u_B, the lateral displacement of the head relative to the axis of the shaft, and a twisting angle ϕ relative to the direction of rod motion are included. In addition, the trajectory of the rod no longer will follow the initial direction of flight, so instead of one parameter p for penetration we employ p as the total length of penetration plus χ, the angle of penetration relative to the original velocity direction. All these quantities are defined in Figs. 10a and 10b.

First, consider the dynamics of the rod itself. The total energy of the rod is

$$T = (M_s + M_f)\left(\frac{1}{2}\, U^2 + \frac{1}{10}\, \dot{u}_B^2\right) + \frac{1}{2}\, I\dot{\phi}^2 \qquad (46)$$

where I is the rod moment of inertia, U is the center of mass velocity of the rod and $\dot{u}_B$ the bending velocity. Since bending and other nonaxial effects are generally small corrections to the total penetration, we treat the rod as a single element, not separating it into head and shaft, for the purpose of calculating these effects.

The variables expressing lateral deflection are then determined by

$$\ddot{\phi} = F_L\, \frac{(L/2)}{I} \qquad (47)$$

where L is the total length of the rod, and

$$\dot{u}_B = \frac{5F_L}{M_s + M_f} \qquad (48)$$

The lateral force F_L is computed in the following way. As the rod impacts a target at an oblique angle, one corner of

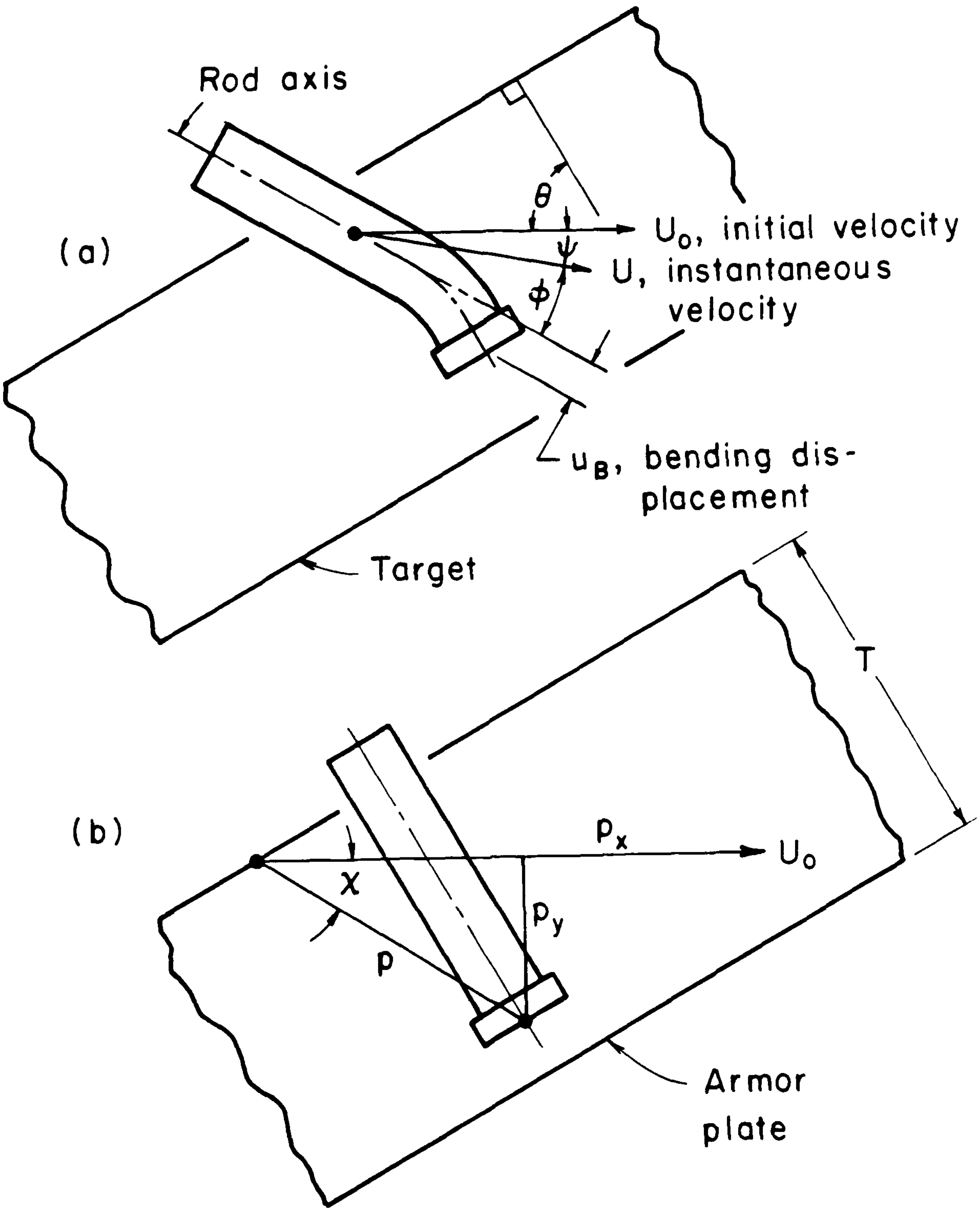
Rod axis
(a)
θ
ψ
φ
U_o, initial velocity
U, instantaneous velocity
u_B, bending displacement
Target
(b)
T
p_x
U_o
χ
p_y
p
Armor plate

Figure 10

the front end first makes contact with the target when the center of the front face of the rod is still a distance

$$d = a \tan \theta$$

from the target, measured in the direction of the rod velocity. We assume the plastic and drag forces acting on the rod begin to increase from zero at this initial instant of contact and rise linearly to their fully-imbedded values when the face of the rod is fully imbedded in the target. The penetration p is measured in the program from this initial contact point. At this point the center of the front face of the rod is a distance $(a \cdot \sin \theta)$ from the target, measured along a normal to the target face. Thus, we treat the target as having an effective thickness $\tau = T + a \sin \theta$, where T is the true target thickness. The total plastic and drag pressure exerted on the head of the rod is computed from (1), and F_A and F_L are found by multiplying this pressure by the front face area and lateral area, respectively, in contact with the target. The head of the rod will begin to widen as soon as the decelerating force of the target acts on it. Full embedding of the head (see Fig. 10) occurs when

$$p = p_o \equiv (a + b) \tan (\theta - \chi) \tag{49}$$

The pressure at the contact interface is

$$\rho_t (E_{*t} + \frac{C_D}{2}(V_f + \dot{\ell}\ )^2)$$

and according to our assumption of a linear initial increase in the contact area, the force exerted on the front face of the rod is

$$F_A = \frac{p}{p_o}\ \pi b^2 \rho_t (E_{*t} + \frac{C_D}{2}(V_f + \dot{\ell})^2),\ p \leq p_o \tag{50}$$

and the force exerted on the side face is

$$F_L = \frac{p}{p_o}\ 4\pi \ell b \rho_t (E_* + \frac{C_D}{2}(V_f + \dot{\ell})^2),\ p \leq p_o \tag{51}$$

We assume this linear increase in contact area holds true up to the point of full embedding at the penetration $p = p_o$. For $p > p_o$, F_L drops to zero since the lateral forces acting on all sides of the head cancel each other, yielding

$$\left.\begin{aligned} F_A &= \pi b^2 \rho_t (E_{*t} + \frac{C_D}{2}(V_f + \dot{\ell})^2) \\ F_L &= 0 \end{aligned}\right\} p > p_o \tag{52}$$

Upon exiting from the backface of the target, the backface model described in the previous section is generalized to oblique exit in the following way. E_{*t} and the drag coefficient C_D near the backface are assumed to decrease according to (45), where the distance from the penetrator to the backface is taken as the projected distance measured normal to the backface. The reduced values of E_* and C_D are substituted directly into the formula for F_A. Near the backface, the projected distance from the center of the rod face to the backface is $\tau - p \cos(\theta - \chi)$, and the expression for the effective E_{*t} corresponding to (45) is

$$E_{*t} = \alpha E_* \tag{53}$$

where α is defined by

$$\alpha = \begin{cases} 1 \quad , & \tau - p\cos(\theta - \chi) \geq \beta r \\ \dfrac{\tau - p\cos(\theta - \chi)}{4\beta} \quad , & \tau - p\cos(\theta - \chi) < \beta r \end{cases} \tag{54}$$

A similar dependence is assumed for C_D near the backface. τ is the effective plate thickness $(T + a \sin\theta)$ measured from the point of initial contact. As the axial force decreases near the backface, the lateral force F_L increases because of the imbalance in the effective E_* of the target on the sides of the head. Therefore, we assume

$$F_L = (1 - \alpha)(4\pi b \ell \rho_t (E_{*t} + \frac{C_D}{2}(V_f + \dot{\ell})^2)) \tag{55}$$

These assumptions completely specify the backface effects for oblique exit from the target.

The equations above, in addition to those described in Section III, are integrated numerically to predict the residual mass, residual velocity, ballistic limit velocity, and other parameters for oblique penetration as well as normal penetration. The oblique model described here has been included in the PEN code, but has not thus far been added to the code ROD. A copy of the code PEN is reproduced in Appendix II. The input parameters which require specification are the geometric dimensions, densities and E_* values of the target and penetrator materials, and the initial striking velocity and olbiquity angle of the penetrator. The output includes ballistic limit velocity or penetration depth, residual mass and residual velocity of the penetrator.

VI. COMPARISON OF EXPERIMENT WITH THEORY

In order to check the programs ROD and PEN against experiment under controlled conditions, several long rods of $L/D = 10$ were fired for us into Rolled Homogeneous Armor targets of Brinell hardness $290\ kg/mm^2$ by the Ballistics Research Lab, Aberdeen Proving Grounds. In order to avoid back-face effects which might modify the effective E_* of the target in these initial experiments, very thick targets of thickness greater than twice the total rod penetration were used. The rods were chosen to provide a variety of materials and strengths, from 1018 steel to soft lead to Mallory 3000, a tungsten alloy. The resulting data were compared to predictions from the ROD and PEN programs to select a best fit value of ε_0, which characterizes the maximum head width, and χ, which relates E_{*d} to the rod strength in Eq. (31). The theoretical values of E_* for the target and penetrator material were used, based on formula (30) and the melting temperature, hardness and heat capacity of the respective materials. The best fit values for ROD were found to be $\varepsilon_0 = 1.36$, $\chi = .42$, and for PEN, $\varepsilon_0 = 1.7$ and $\chi = 1.0$.

A comparison of the resultant theoretical predictions with experiment for the code ROD is shown in Figs. 11 through 13. The corresponding fit to the data for the code PEN is shown in Fig. 14. The high velocity lead rod deformed upon exit from the gun barrel and had a highly irregular shape and $L/D \sim 5$ upon impact at the target. We have used $L/D = 5$ in computing the theoretical penetration for this data point. Agreement with experiment in all cases is within about 15%.

Next, the code was tested for rods against finite thickness targets at normal incidence. The values of the parameters χ and ε_0 found above were kept the same. In the numerical code this set of experiments amounts to a test of the accuracy of the backface model, presented in Section IV. The ballistic limit velocity V_{BL} was determined in the code by incrementally raising the striking velocity of the rod until penetration was

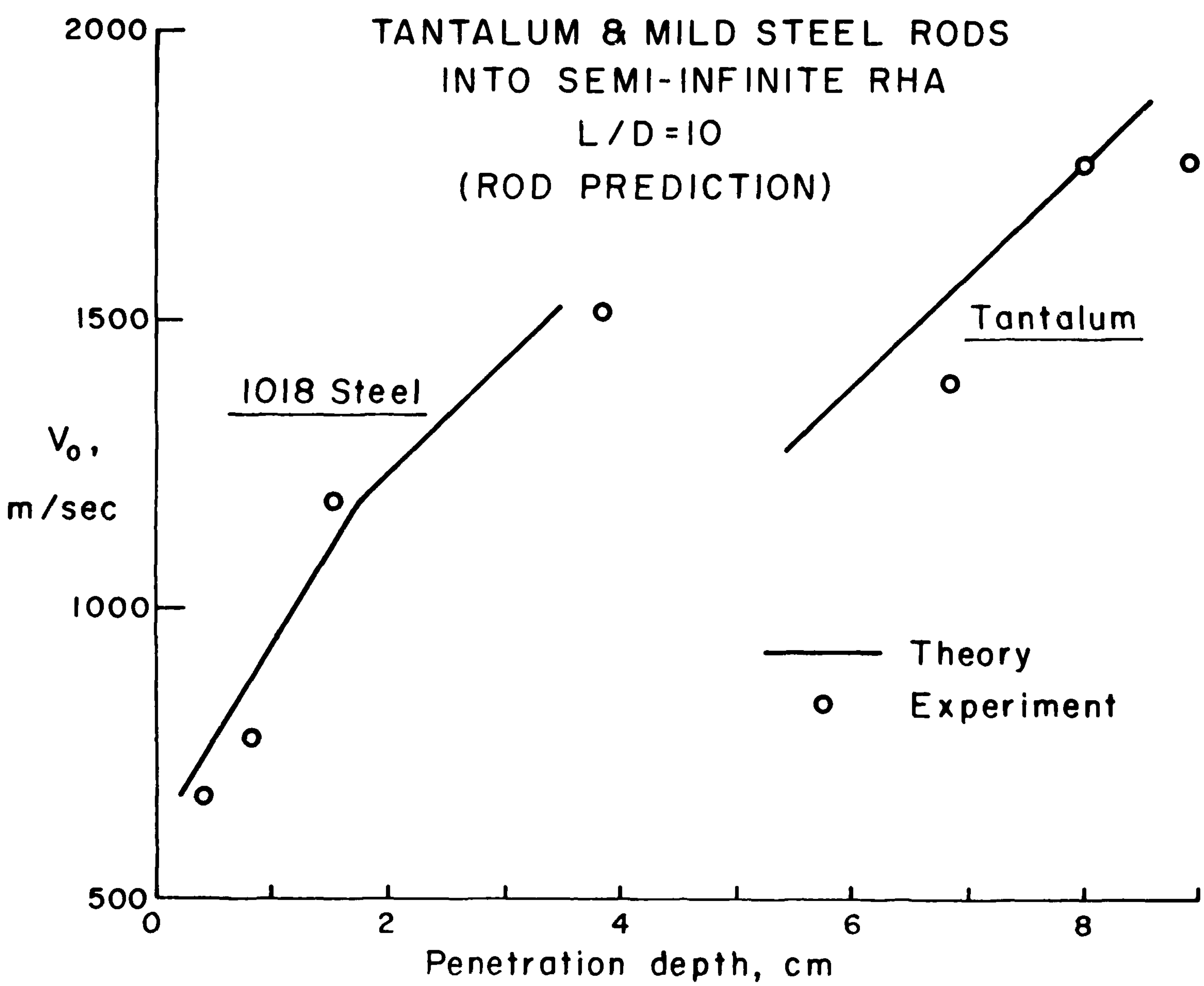
TANTALUM & MILD STEEL RODS
INTO SEMI-INFINITE RHA
L/D=10
(ROD PREDICTION)
2000
1500
1000
500
V_0,
m/sec
1018 Steel
Tantalum
Theory
Experiment
0
2
4
6
8
Penetration depth, cm

Figure 11

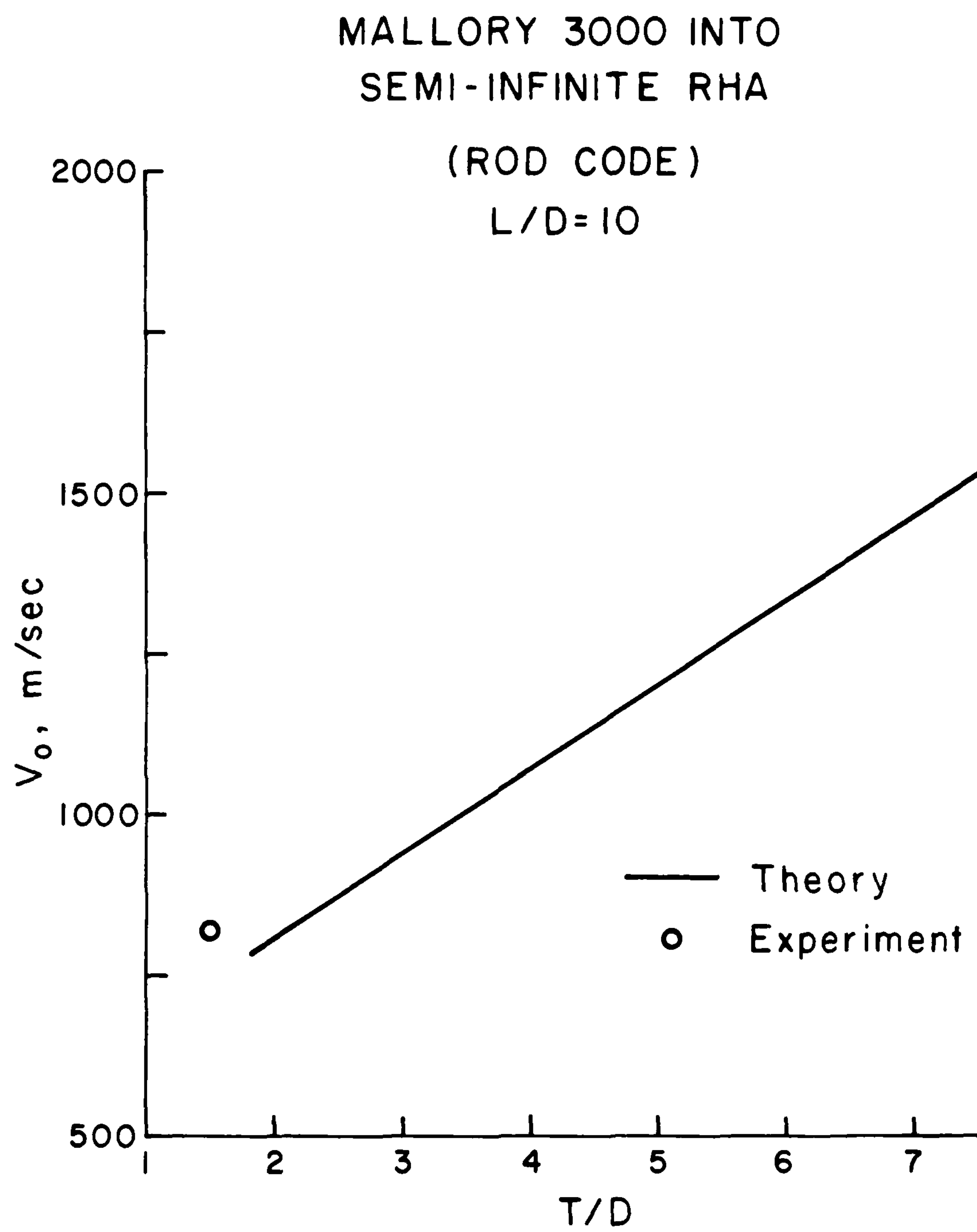
MALLORY 3000 INTO
SEMI-INFINITE RHA
(ROD CODE)
L/D=10
2000
1500
1000
500
V_o, m/sec
1
2
3
4
5
6
7
8
T/D
Theory
Experiment

Figure 12

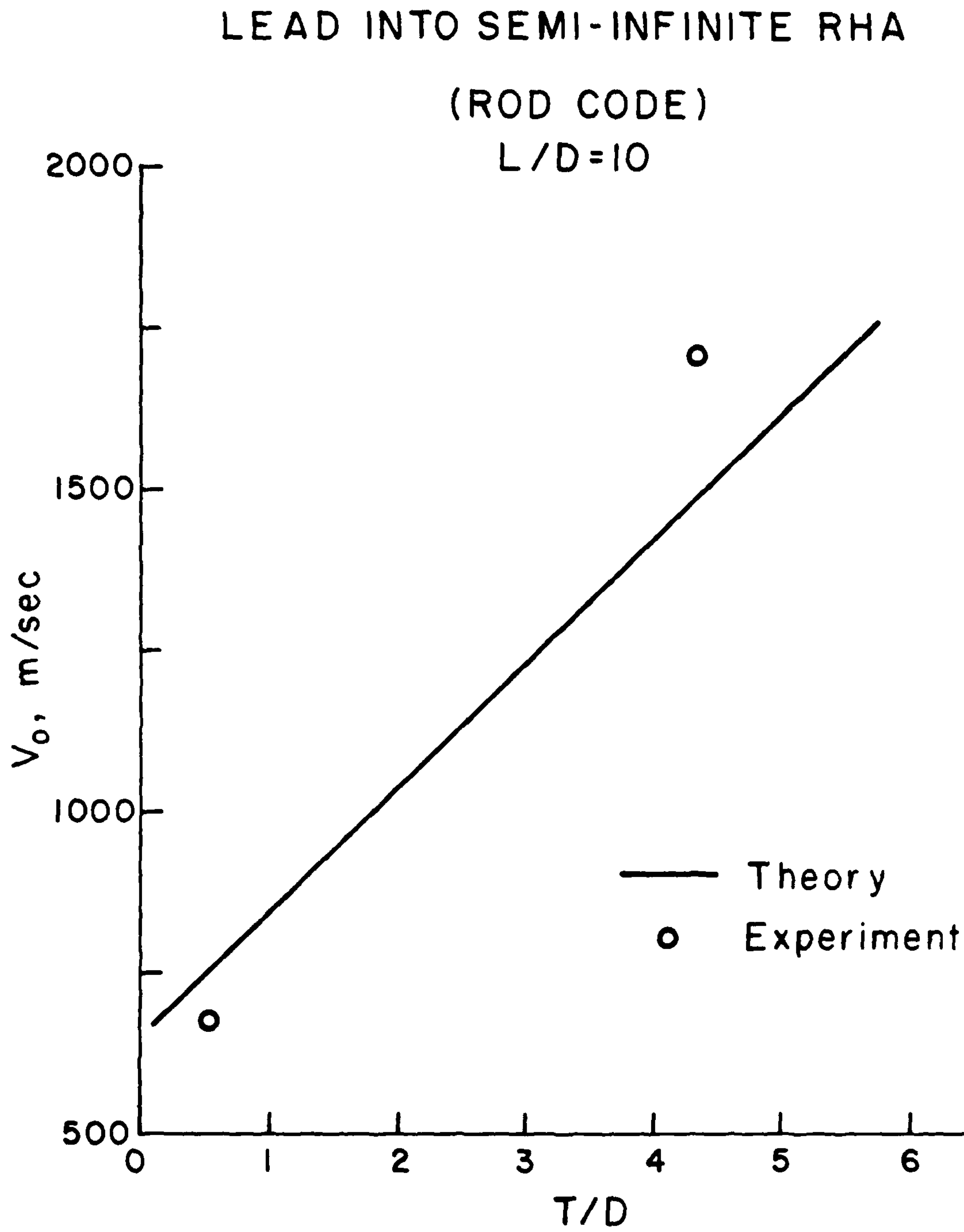
LEAD INTO SEMI-INFINITE RHA
(ROD CODE)
L/D=10
2000
1500
1000
500
V_o, m/sec
0
1
2
3
4
5
6
7
T/D
Theory
Experiment

Figure 13

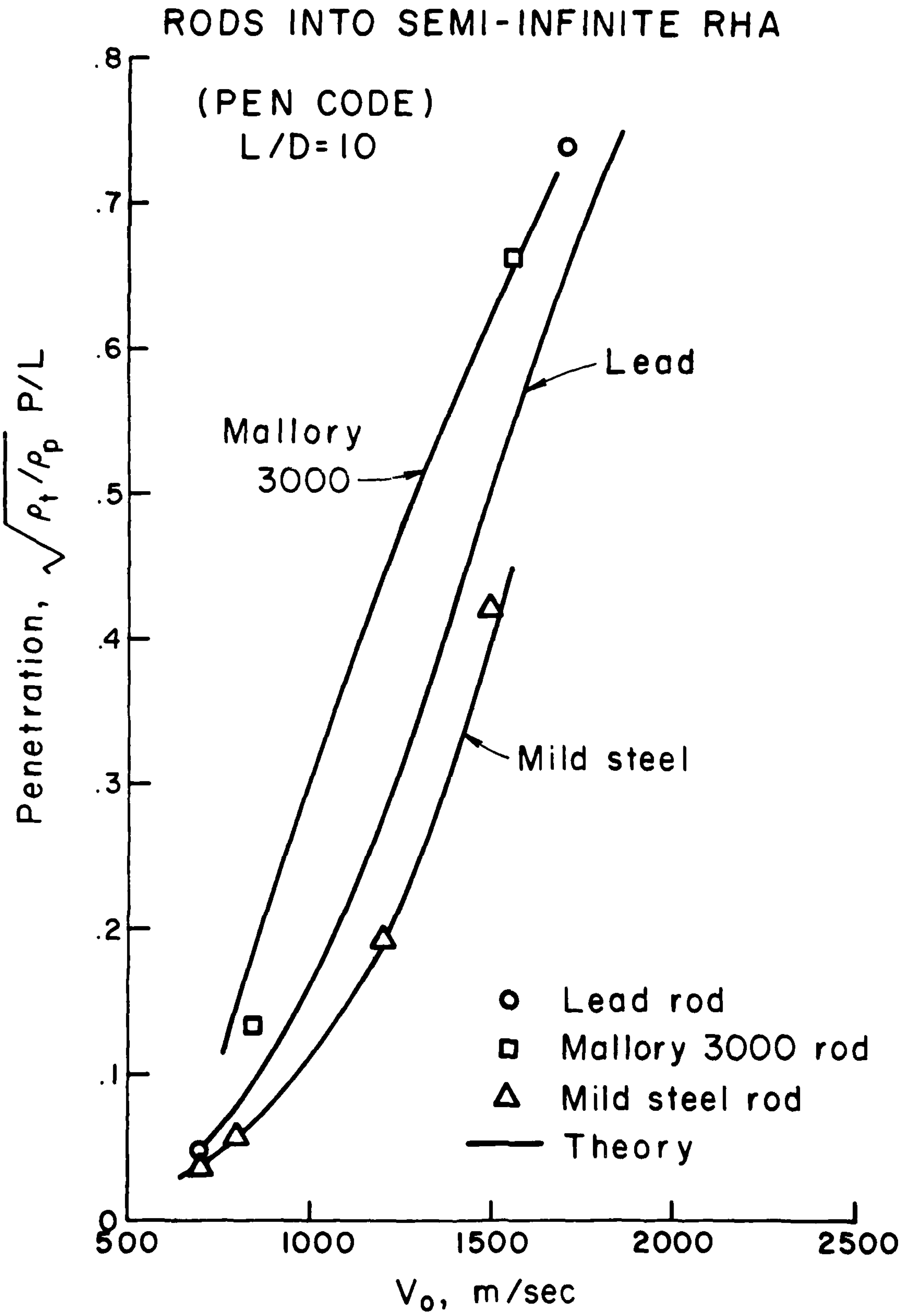

RODS INTO SEMI-INFINITE RHA
(PEN CODE)
L/D=10
Lead
Mallory 3000
Mild steel
Lead rod
Mallory 3000 rod
Mild steel rod
Theory
Penetration, $\sqrt{\rho_t/\rho_p}$ P/L
V_o, m/sec
0
.1
.2
.3
.4
.5
.6
.7
.8
500
1000
1500
2000
2500

Figure 14

achieved. This theoretical V_{BL} from the ROD code was compared to one set of experiments (Lambert[9]) with 65 gm Bearcat steel rods of $L/D = 5$, 10 and 20 into RHA targets of various hardness from BHN = 260 to 375 kg/mm^2. These date are presented in Figs. 15 through 17. Agreement is excellent, although there is a slight tendency for the higher L/D rod to overpenetrate and the lower L/D rod to underpenetrate. In Figs. 18 through 20 these data of Lambert are plotted in dimensionless form against another set of experiments (Herr[10]) in which 1.94, 3.89, and 7.78 gram Bearcat steel rods were fired into RHA plates which were annealed to a Brinell hardness of 400. In Figs. 18 through 20 the plate thickness is expressed in units of T/D or (thickness)/(rod diameter), since it is the rod width D that sets the dimension for backface effects. It is apparent in the figures that the two sets of experimental data do not overlap, particularly for $L/D = 10$ and 20. This can be shown to be a result of the different Brinell hardnesses of the armor targets used in the two sets of experiments.[11] Note, for example, that the 1.94, 3.89 and 7.78 gram rods do fall on the same ballistic curve. In Herr's experiments, all targets were heat treated to a uniform hardness of BHN = 400. Thus, they all had the same value of E_*, about 215 Btu/lb. In Lambert's data, the Brinell hardness varies from about 260 to 375 km/mm^2 with corresponding values of E_* ranging from 170 to 210 Btu/lb. The theoretical curves corresponding to these two sets of E_* values are plotted in Figs. 18 through 20, where the average E_* of Lambert's targets, 190 Btu/lb, is used. The theory clearly shows the same shift in V_{BL} with hardness that is seen in the experimental data. Thus, the different values of E_* corresponding to different Brinell hardnesses, as predicted by Eq. (30), account for the apparent failure of scaling in the data. This set of experiments provides a sensitive test of the ability of the Integral Theory to predict the effect of materials properties, such as hardness, on penetration and ballistic limit.

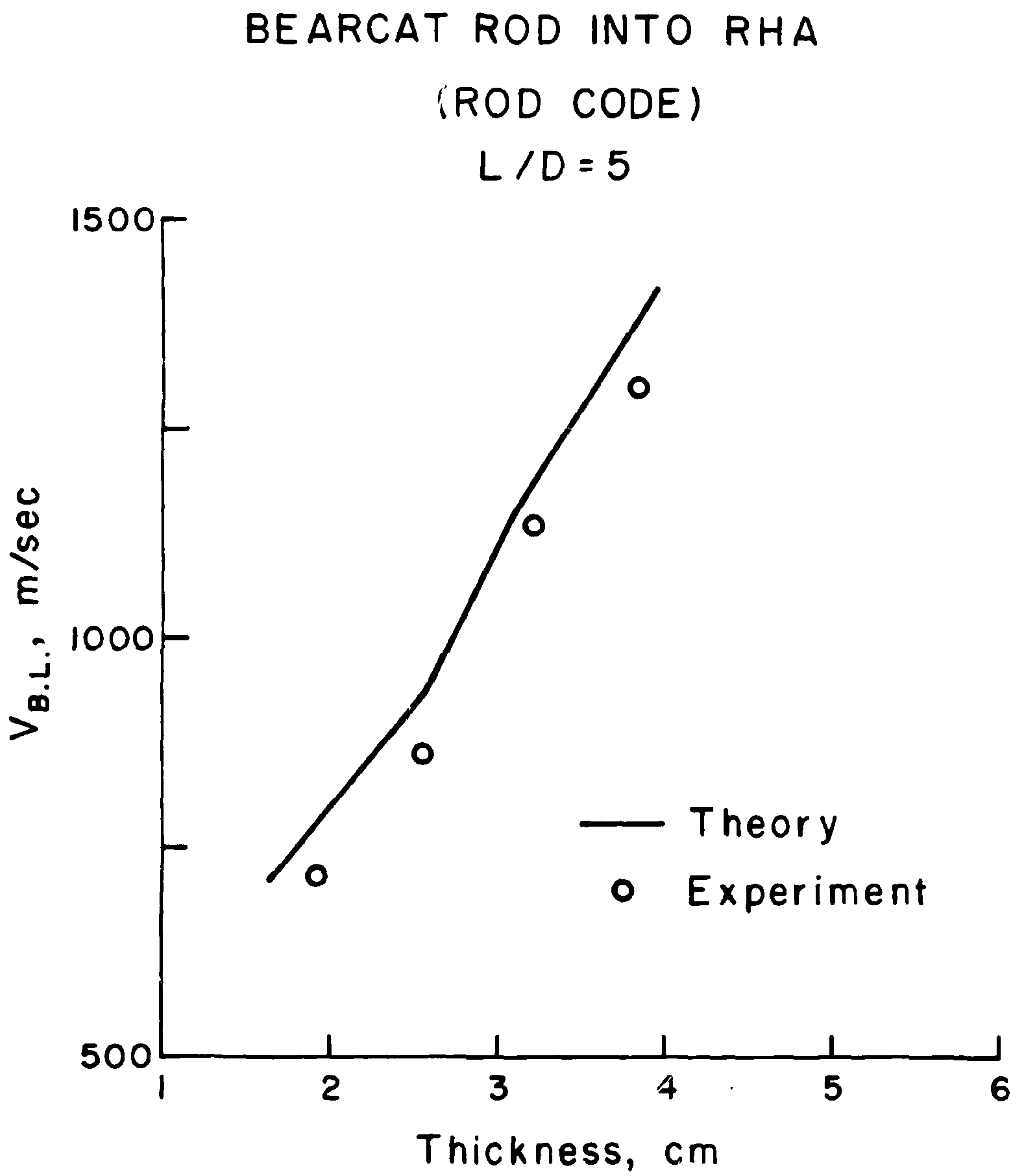
BEARCAT ROD INTO RHA
(ROD CODE)
L/D=5
1500
1000
500
$V_{B.L.}$, m/sec
1
2
3
4
5
6
Thickness, cm
Theory
Experiment

Figure 15

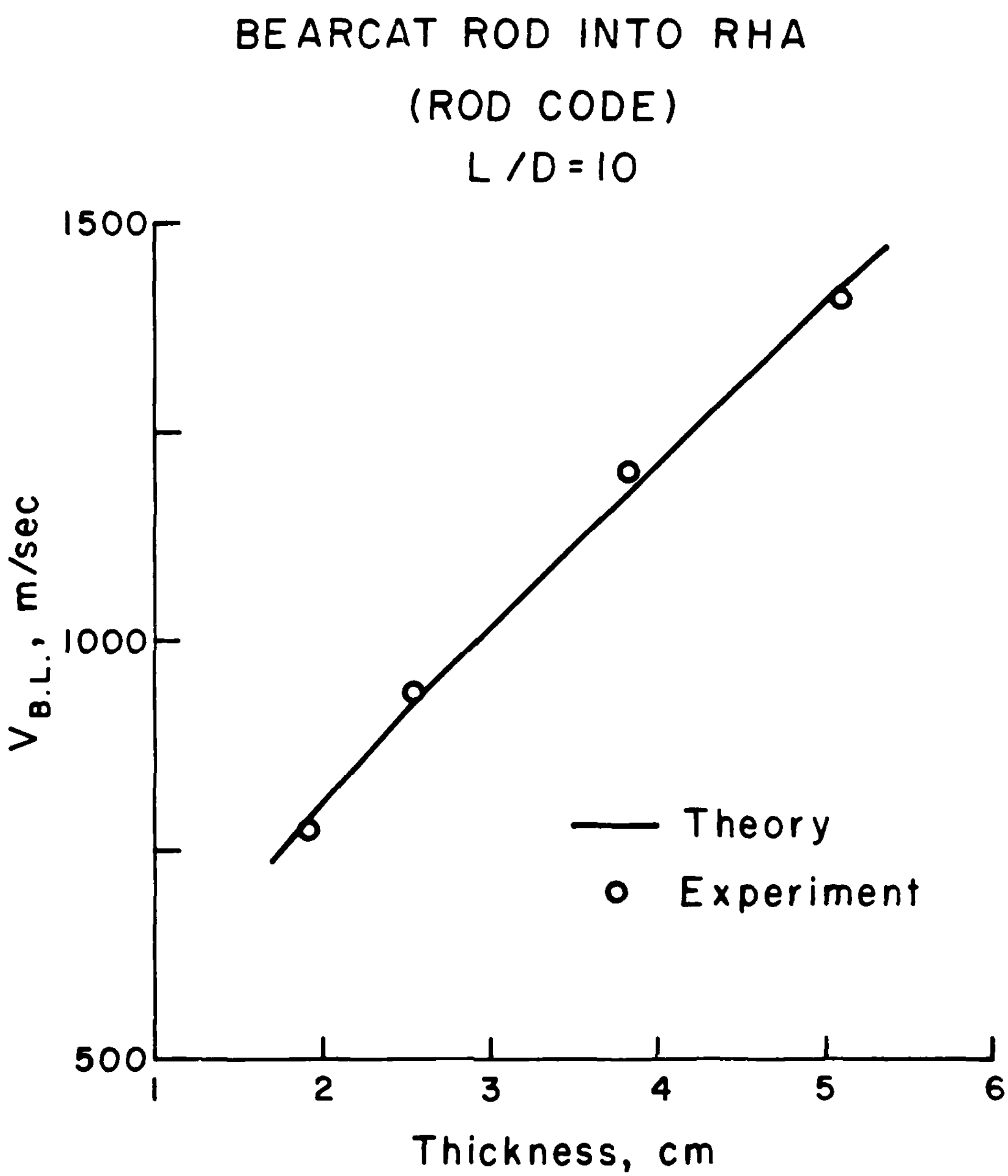
BEARCAT ROD INTO RHA
(ROD CODE)
L/D = 10
1500
1000
500
$V_{B.L.}$, m/sec
1
2
3
4
5
6
Thickness, cm
Theory
Experiment

Figure 16

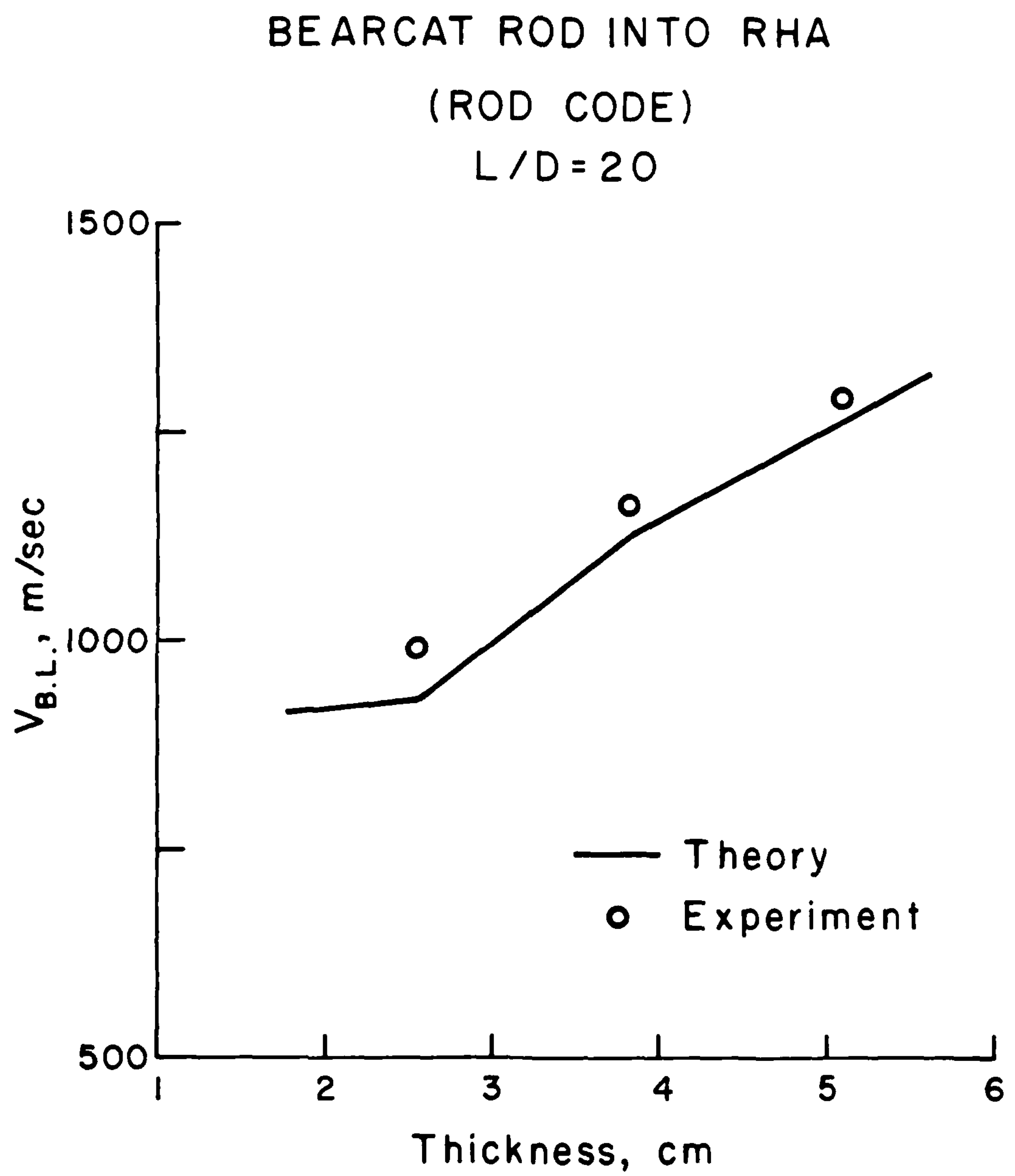
BEARCAT ROD INTO RHA
(ROD CODE)
L/D=20
1500
1000
500
$V_{B.L.}$, m/sec
1
2
3
4
5
6
Thickness, cm
Theory
Experiment

Figure 17

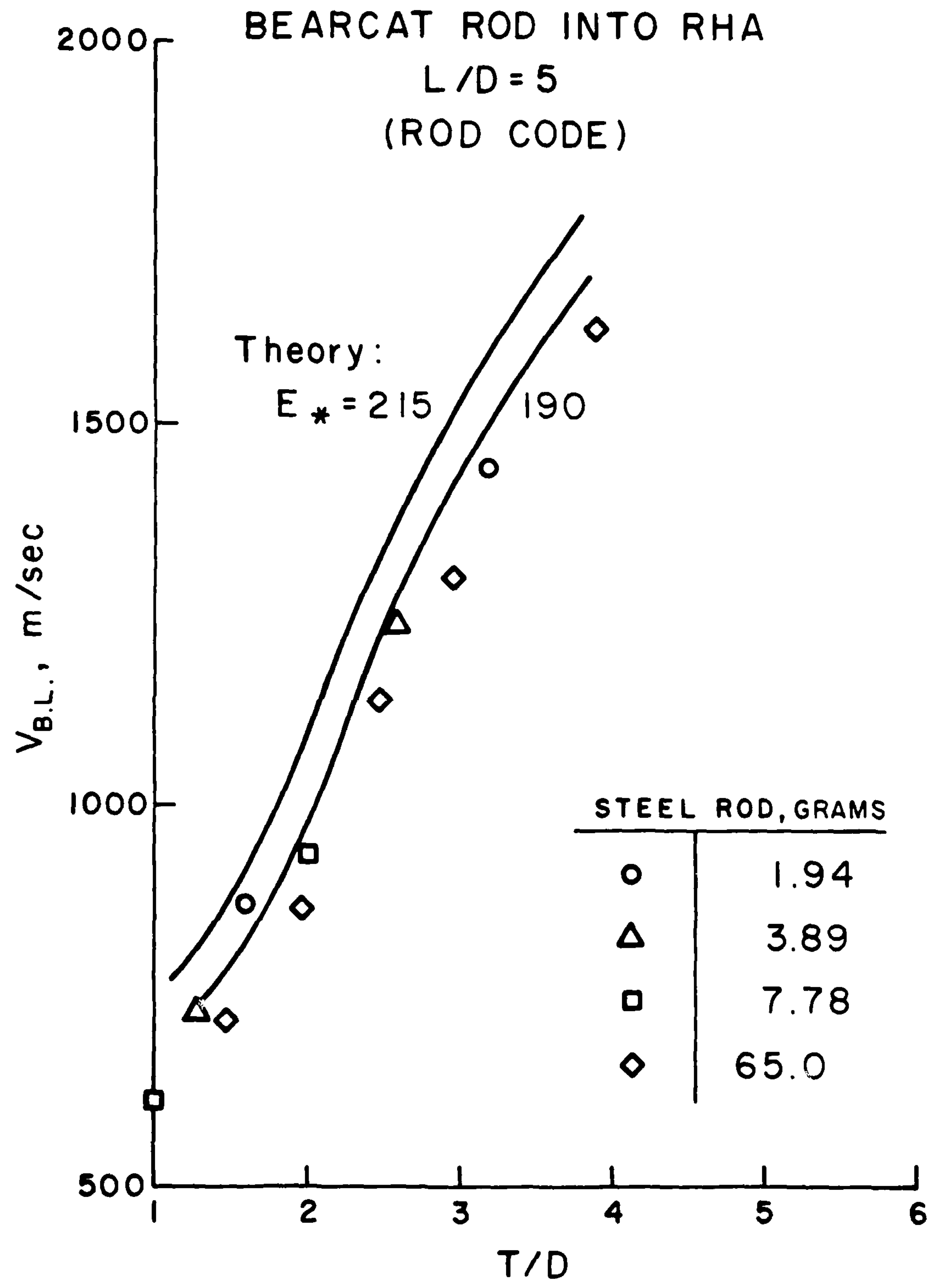

BEARCAT ROD INTO RHA
L/D = 5
(ROD CODE)
2000
1500
1000
500
$V_{B.L.}$, m/sec
Theory:
E_* = 215
190
STEEL ROD, GRAMS
1.94
3.89
7.78
65.0
1
2
3
4
5
6
T/D

Figure 18

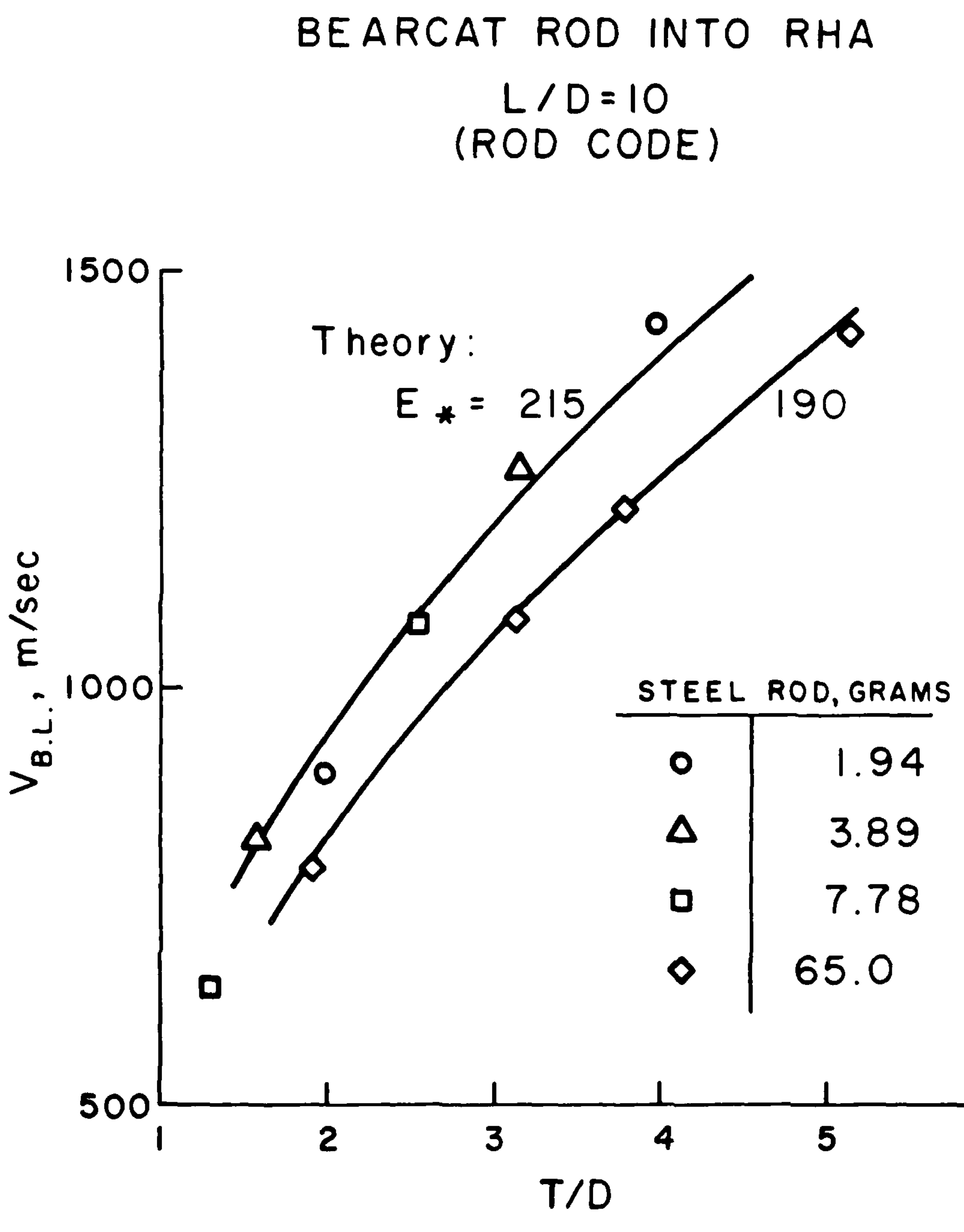
BEARCAT ROD INTO RHA
L/D=10
(ROD CODE)
Theory:
E* = 215
190
STEEL ROD, GRAMS
1.94
3.89
7.78
65.0
V B.L., m/sec
1500
1000
500
1
2
3
4
5
6
T/D

Figure 19

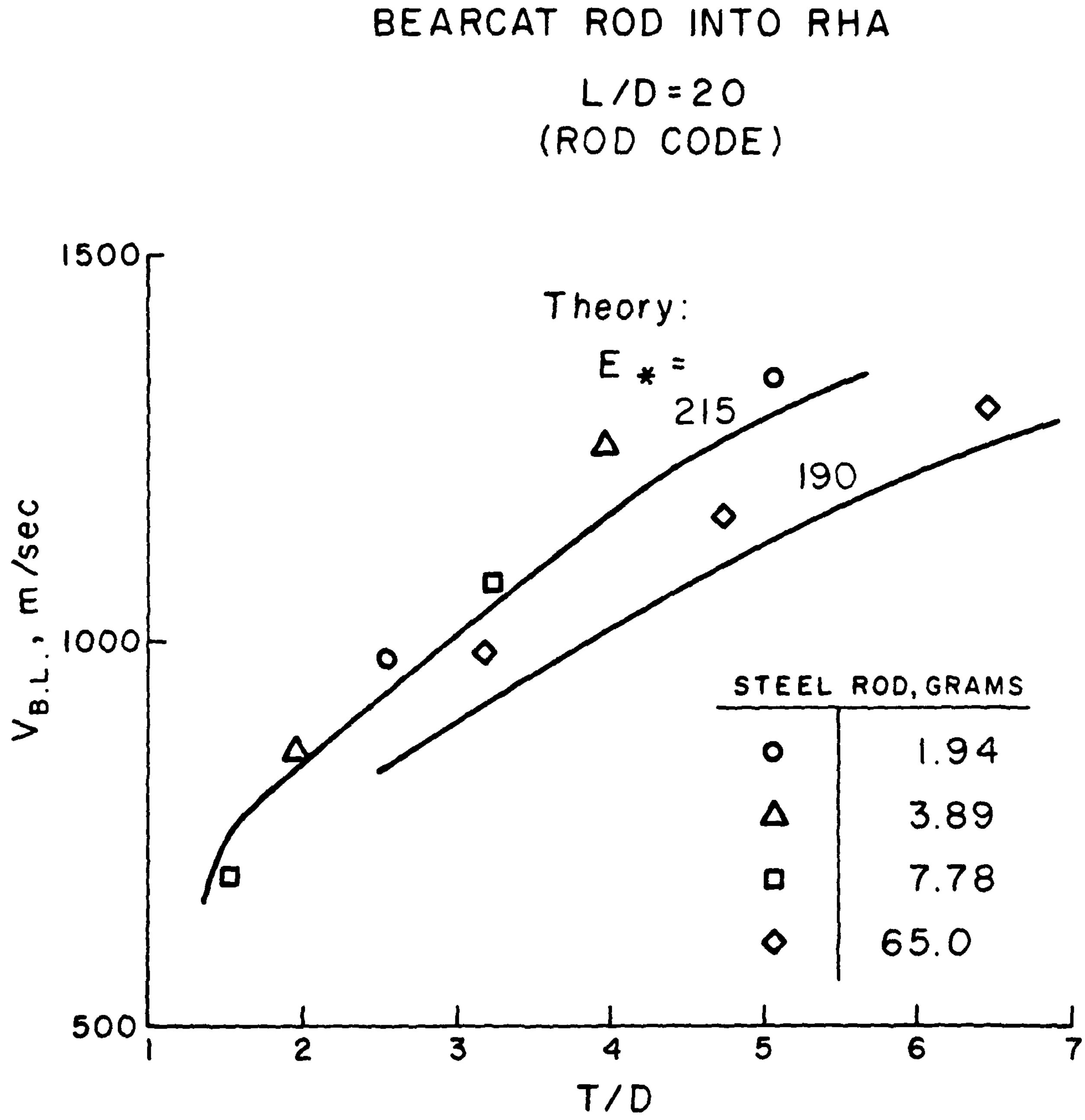
BEARCAT ROD INTO RHA
L/D = 20
(ROD CODE)
Theory:
E * =
215
190
STEEL ROD, GRAMS
1.94
3.89
7.78
65.0
1500
1000
500
V B.L. , m/sec
1
2
3
4
5
6
7
T/D

Figure 20

In Figs. 21 through 24 the theoretical value of the residual mass M_R versus striking velocity is compared to experiment[9,10] for Bearcat steel and Mallory 3000 rods. The residual mass computed in the program is the sum of the mass of the head and shaft of the rod at the instant the target backface is reached. Although there is a fair amount of scatter in the data, good qualitative agreement is attained over the range of velocities and target thicknesses in the experiment. In Figs. 25 through 29 the predicted residual velocity of the rod fragment is compared with experiment for various thickness targets and rods of various L/D, for Mallory 3000 as well as steel. These comparisons are typical. The agreement is good between the code and experiment to about ±15%.

In Figs. 30 and 31 typical oblique rod shots[9] are compared to the PEN code prediction. The ballistic limit is plotted versus striking velocity for Bearcat rods into RHA at 60° incidence. Again, the agreement between theory and experiment is good to better than 10%.

In order to provide further confirmation of the numerical codes, especially over a wider range of materials, published data were obtained for long rods (wires) of gold, tin, aluminum, and magnesium fired into 7075-T6 Aluminum semi-infinite targets.[6] The values of E_* for the targets and penetrators were obtained from handbook data on the materials involved, and substituted into formula (30). The resulting values of E_* are displayed in Fig. 32, together with the experimental and theoretical curves of penetration versus velocity for the four rod materials. The penetration is normalized to allow presentation of all curves on the same graph. The very good agreement over a range of rod density from 1.8 to 19 gm/cc confirms that density variations are taken into account correctly in the code.

As yet another test of the influence of the material hardness on penetration, published data[7] for steel and Densimet 17 rods fired into various types of semi-infinite steel targets

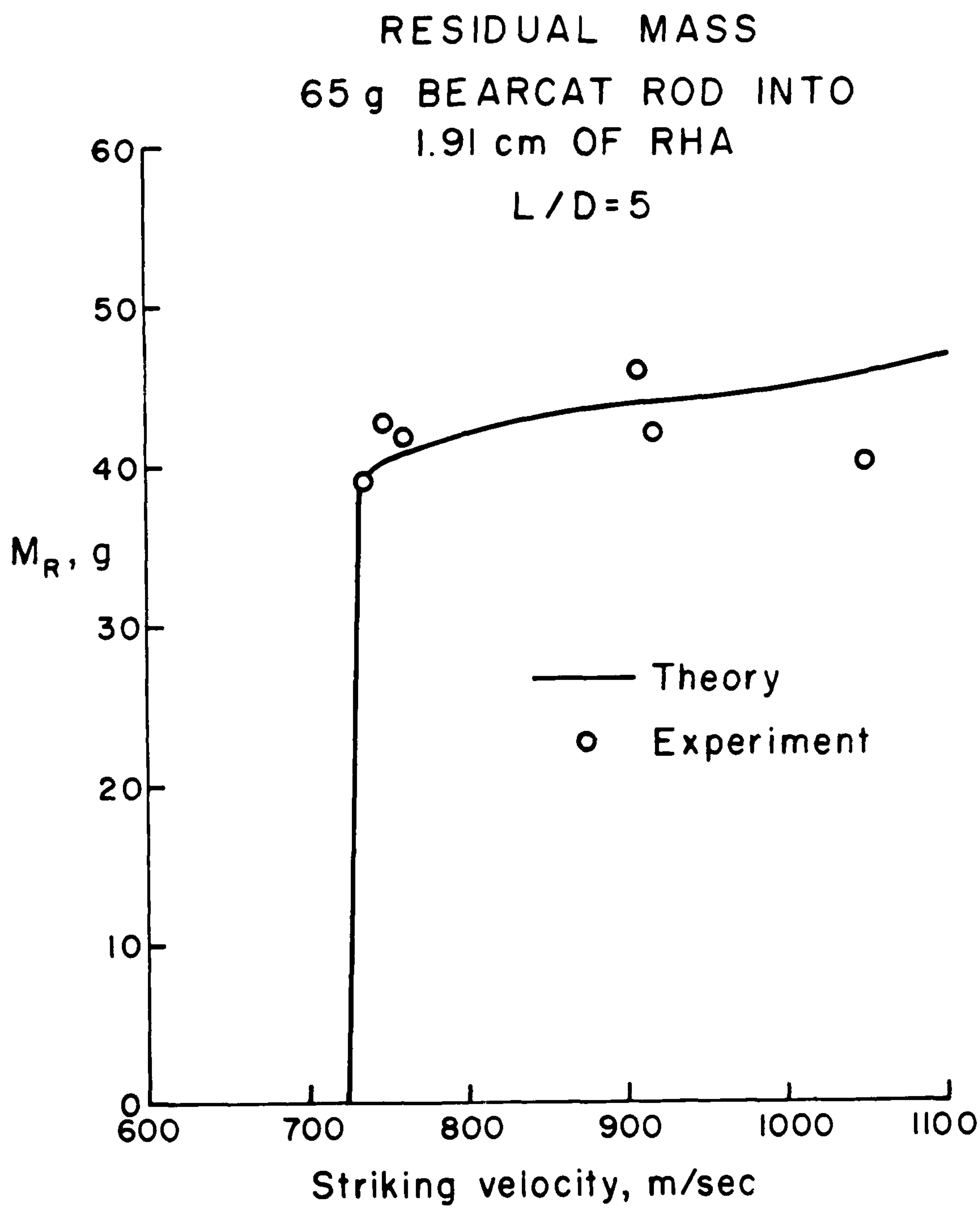
RESIDUAL MASS
65 g BEARCAT ROD INTO
1.91 cm OF RHA
L/D=5
60
50
40
30
20
10
0
M_R, g
Theory
Experiment
600
700
800
900
1000
1100
Striking velocity, m/sec

Figure 21

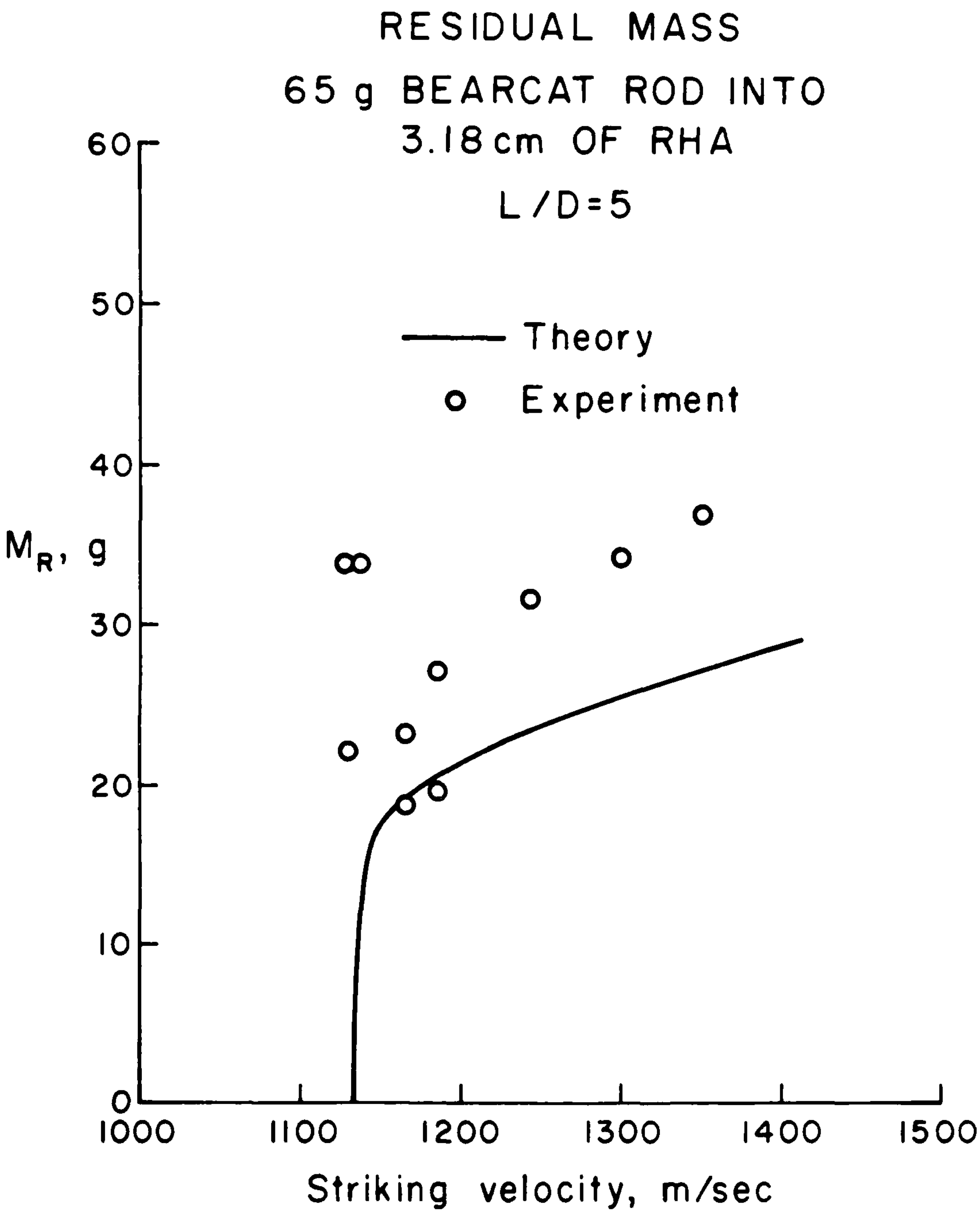
RESIDUAL MASS
65 g BEARCAT ROD INTO
3.18 cm OF RHA
L/D=5
Theory
Experiment
M_R, g
60
50
40
30
20
10
0
1000
1100
1200
1300
1400
1500
Striking velocity, m/sec

Figure 22

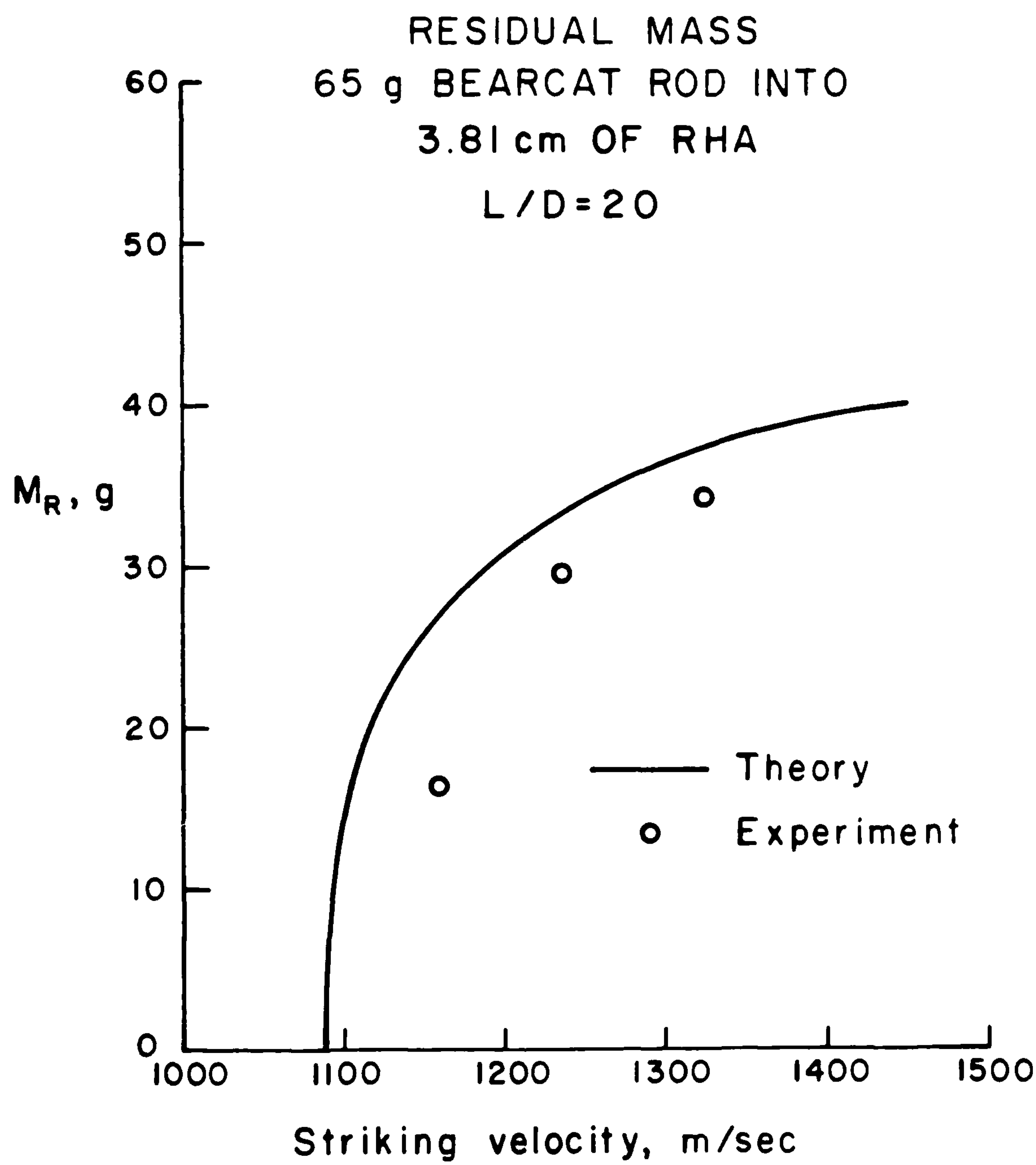
RESIDUAL MASS
65 g BEARCAT ROD INTO
3.81 cm OF RHA
L/D=20
60
50
40
30
20
10
0
M_R, g
1000
1100
1200
1300
1400
1500
Striking velocity, m/sec
Theory
Experiment

Figure 23

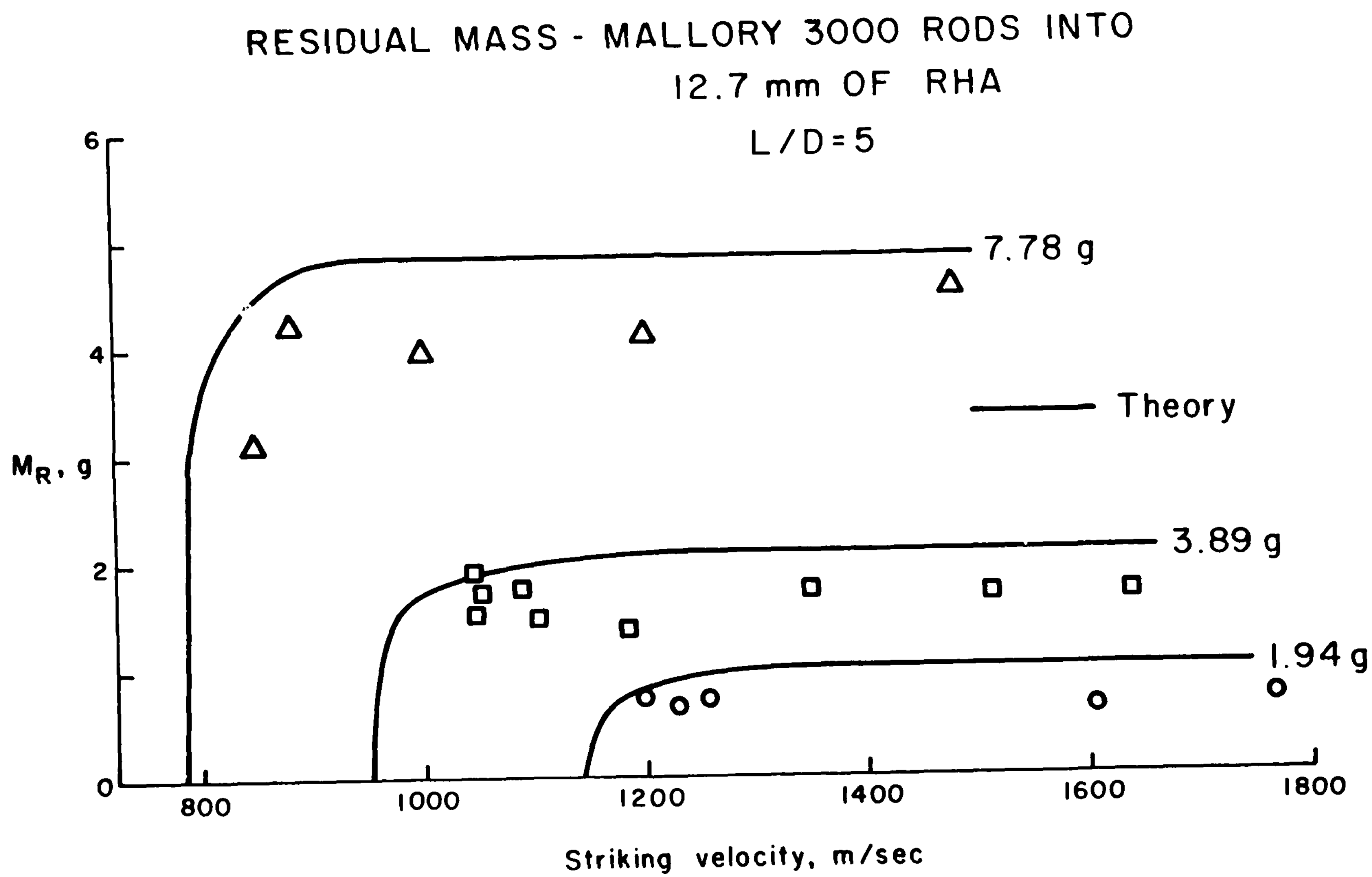
RESIDUAL MASS - MALLORY 3000 RODS INTO
12.7 mm OF RHA
L/D=5
7.78 g
Theory
3.89 g
1.94 g
M_R, g
6
4
2
0
800
1000
1200
1400
1600
1800
Striking velocity, m/sec

Figure 24

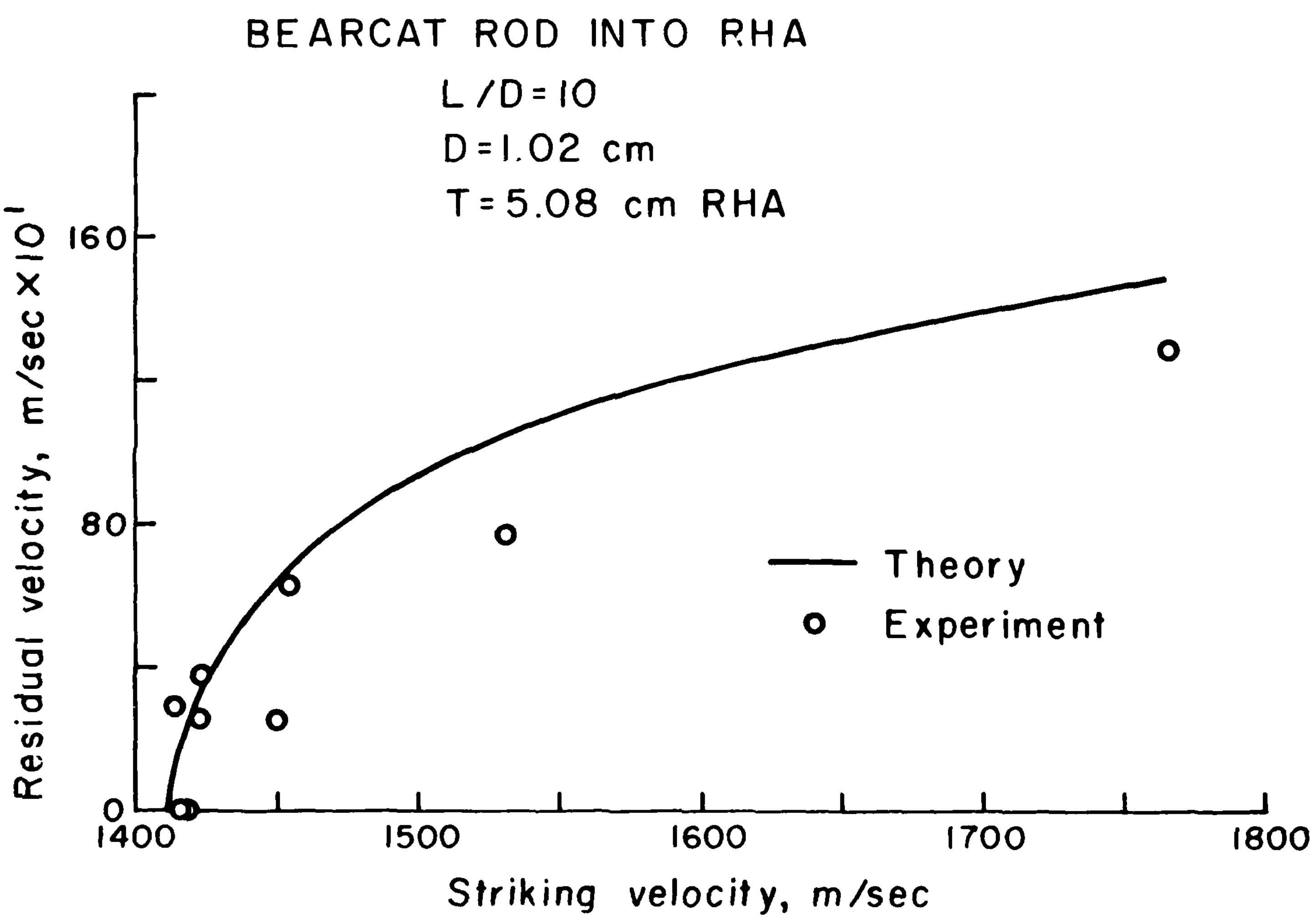
BEARCAT ROD INTO RHA
L/D=10
D=1.02 cm
T=5.08 cm RHA
Residual velocity, m/sec X10[1]
160
80
0
1400
1500
1600
1700
1800
Striking velocity, m/sec
Theory
Experiment

Figure 25

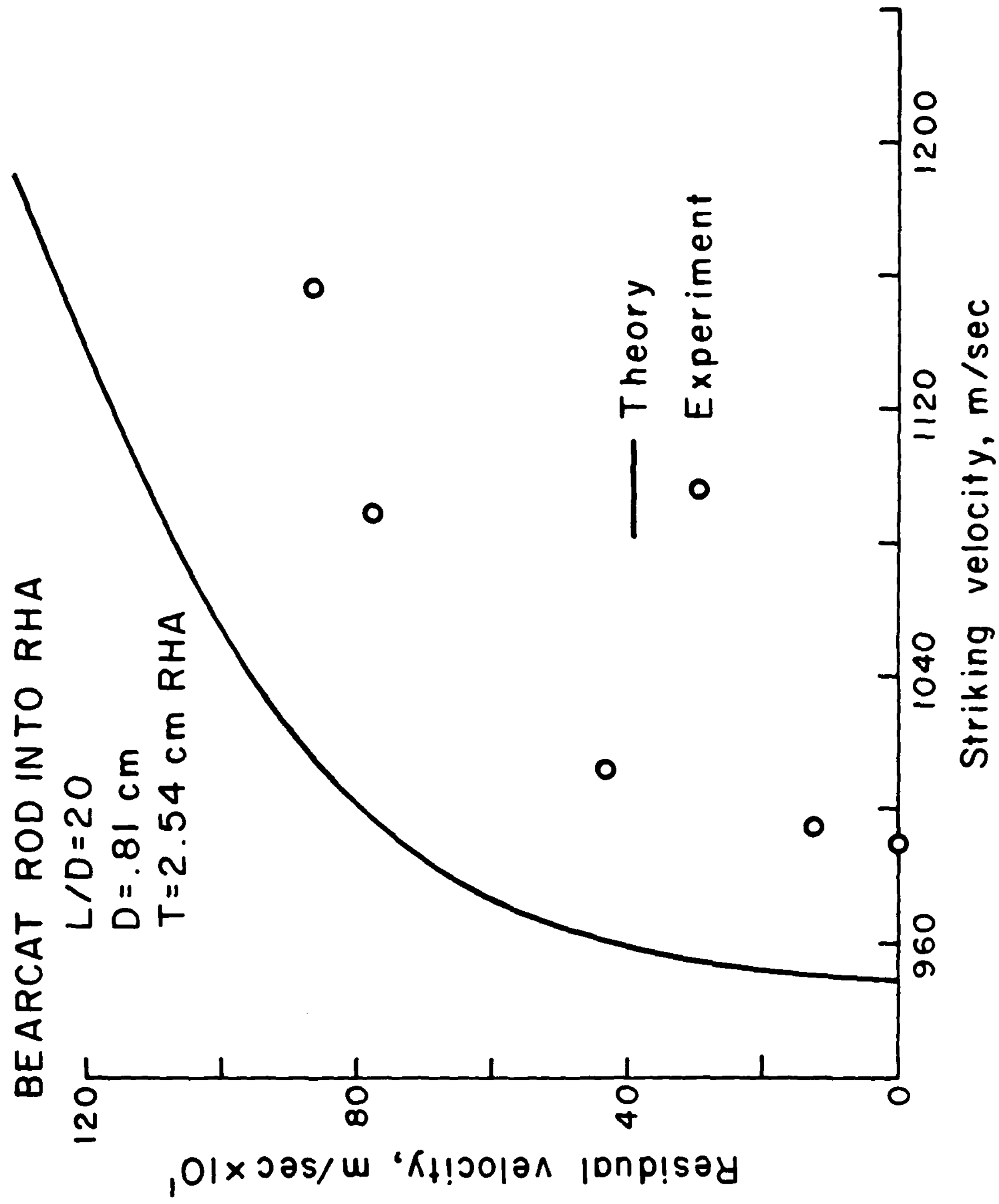

BEARCAT ROD INTO RHA
L/D=20
D=.81 cm
T=2.54 cm RHA
Theory
Experiment
Residual velocity, m/sec x10[1]
120
80
40
0
960
1040
1120
1200
Striking velocity, m/sec

Figure 26

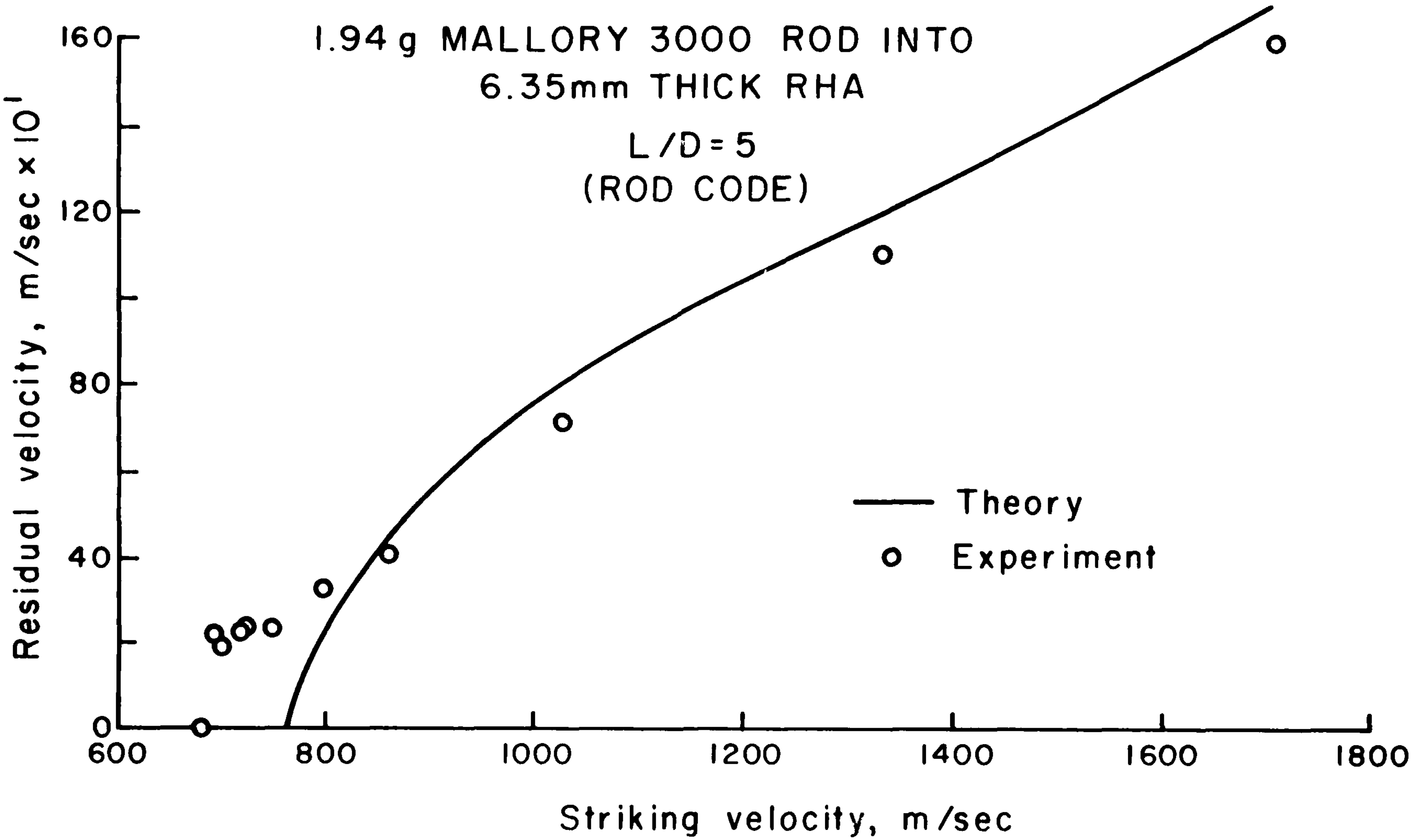
1.94 g MALLORY 3000 ROD INTO
6.35mm THICK RHA
L/D = 5
(ROD CODE)
Theory
Experiment
Residual velocity, m/sec x 10¹
Striking velocity, m/sec
0
40
80
120
160
600
800
1000
1200
1400
1600
1800

Figure 27

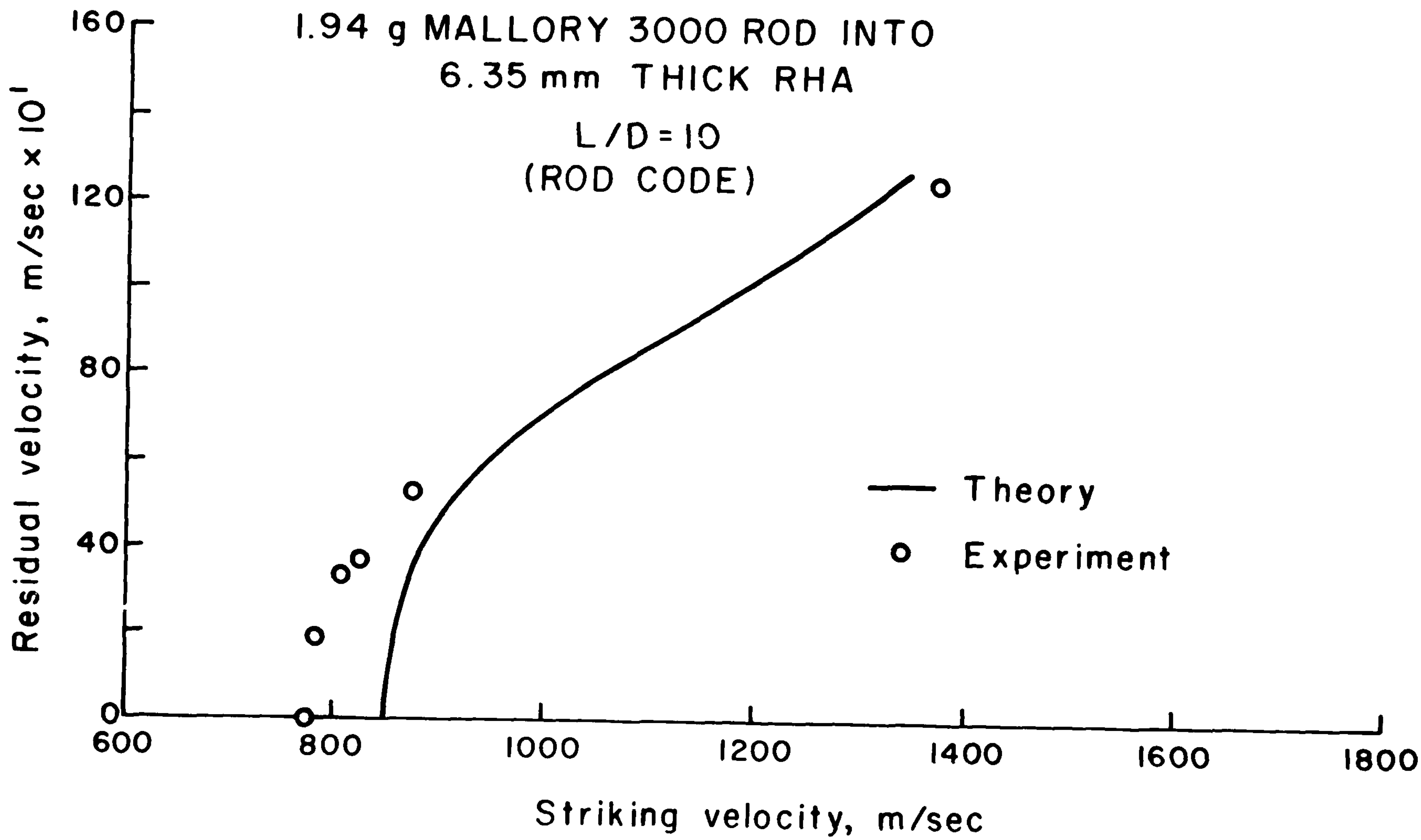
1.94 g MALLORY 3000 ROD INTO
6.35 mm THICK RHA
L/D = 10
(ROD CODE)
Theory
Experiment
Residual velocity, m/sec x 10¹
Striking velocity, m/sec
160
120
80
40
0
600
800
1000
1200
1400
1600
1800

Figure 28

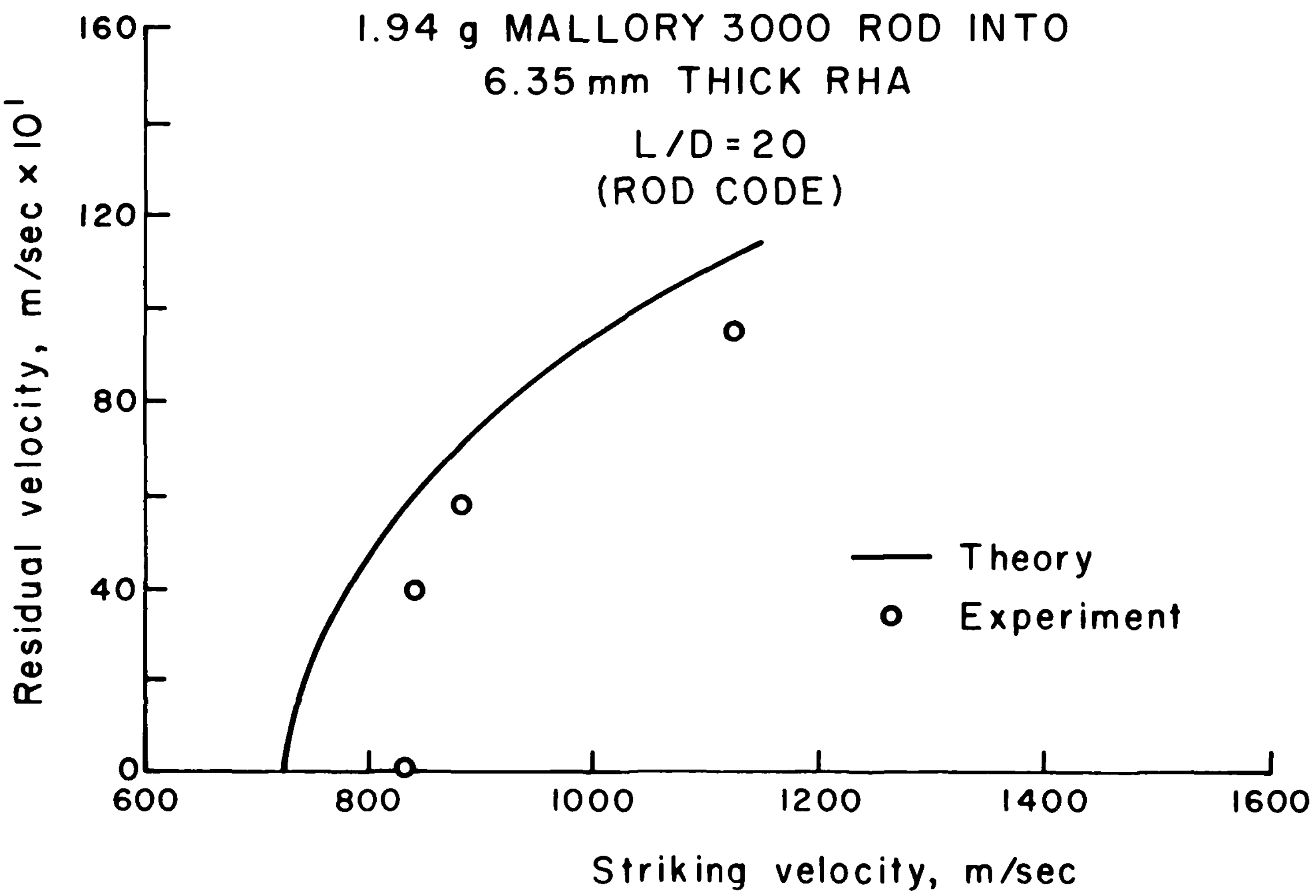
1.94 g MALLORY 3000 ROD INTO
6.35 mm THICK RHA
L/D = 20
(ROD CODE)
Theory
Experiment
160
120
80
40
0
600
800
1000
1200
1400
1600
Residual velocity, m/sec × 10[1]
Striking velocity, m/sec

Figure 29

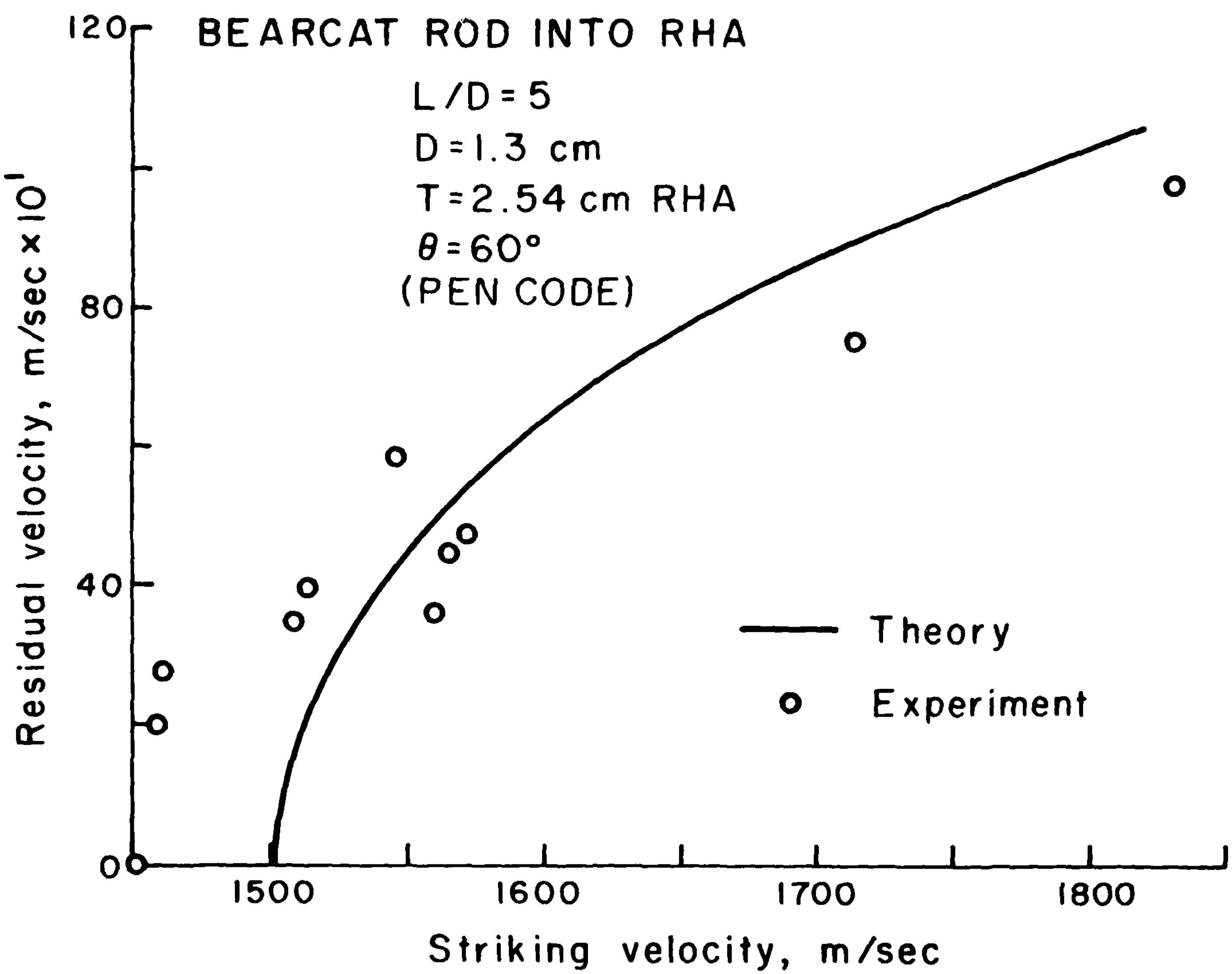

BEARCAT ROD INTO RHA
L/D=5
D=1.3 cm
T=2.54 cm RHA
θ=60°
(PEN CODE)
Theory
Experiment
120
80
40
0
0
1500
1600
1700
1800
Residual velocity, m/sec x 10^1
Striking velocity, m/sec

Figure 30

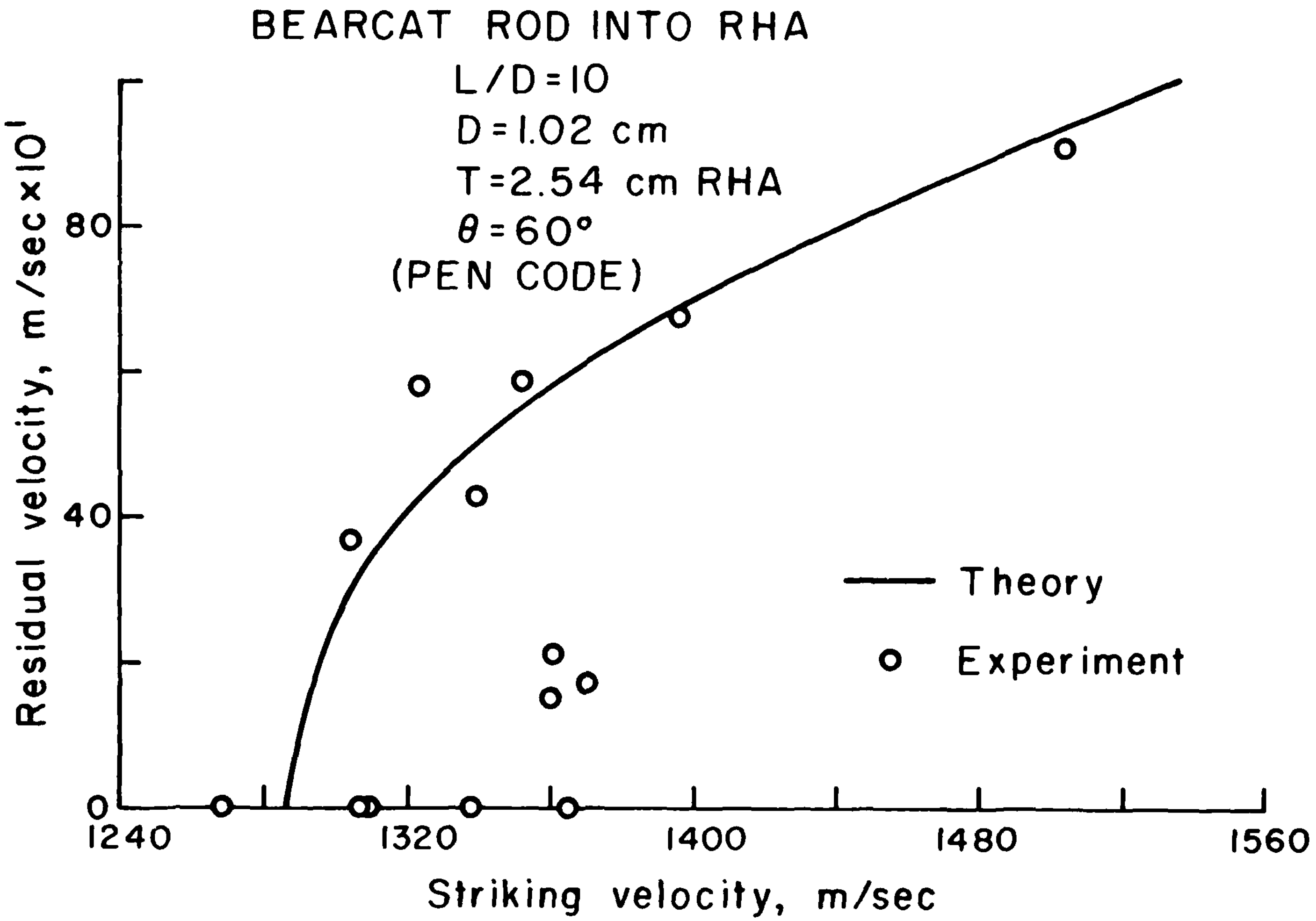
BEARCAT ROD INTO RHA
L/D=10
D=1.02 cm
T=2.54 cm RHA
θ=60°
(PEN CODE)
Residual velocity, m/sec x10¹
0
40
80
1240
1320
1400
1480
1560
Striking velocity, m/sec
Theory
Experiment

Figure 31

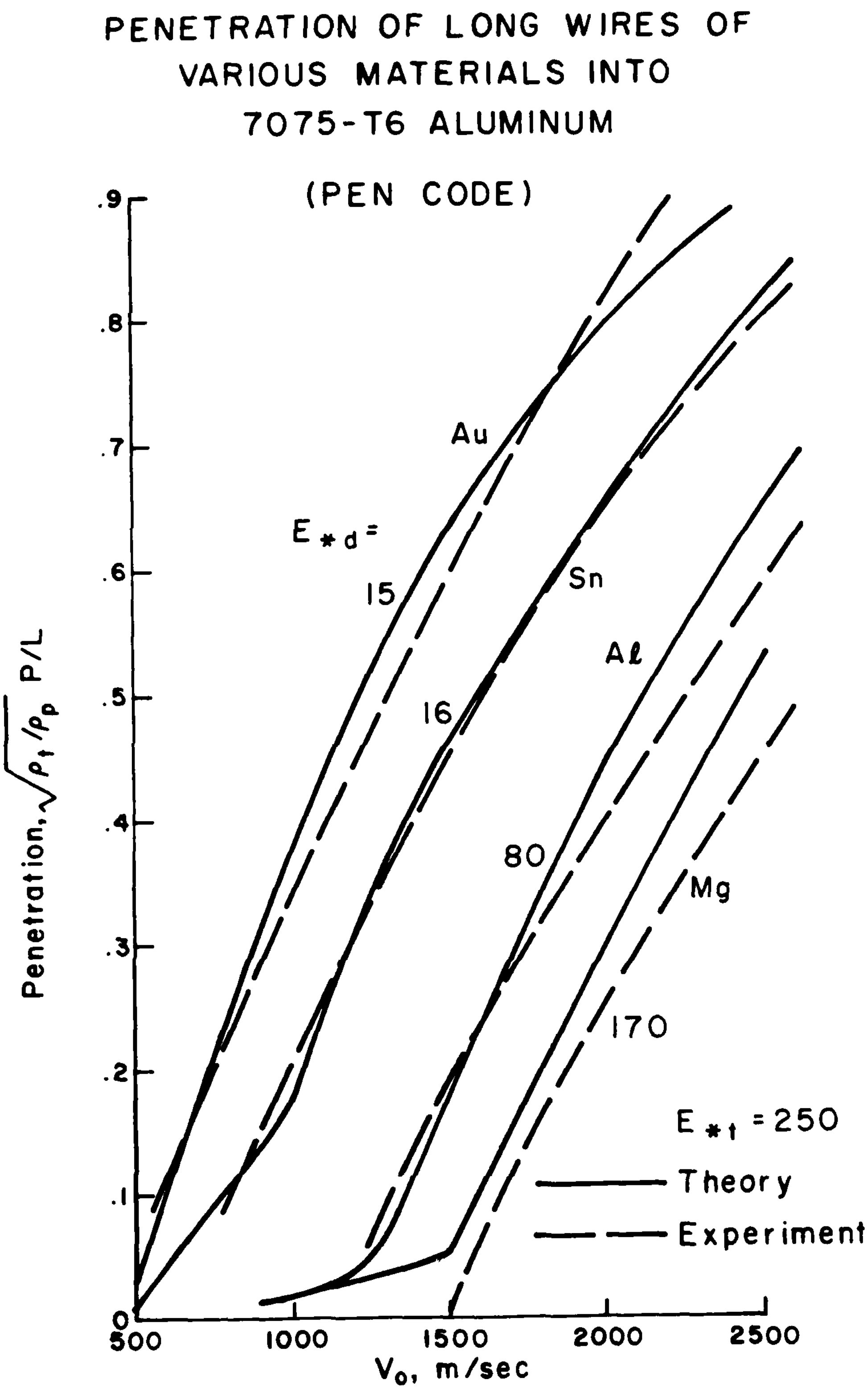

PENETRATION OF LONG WIRES OF VARIOUS MATERIALS INTO 7075-T6 ALUMINUM
(PEN CODE)
Penetration, $\sqrt{\rho_t/\rho_p}$ P/L
V_o, m/sec
Au
Sn
Al
Mg
E_{*d} =
15
16
80
170
E_{*t} = 250
Theory
Experiment

Figure 32

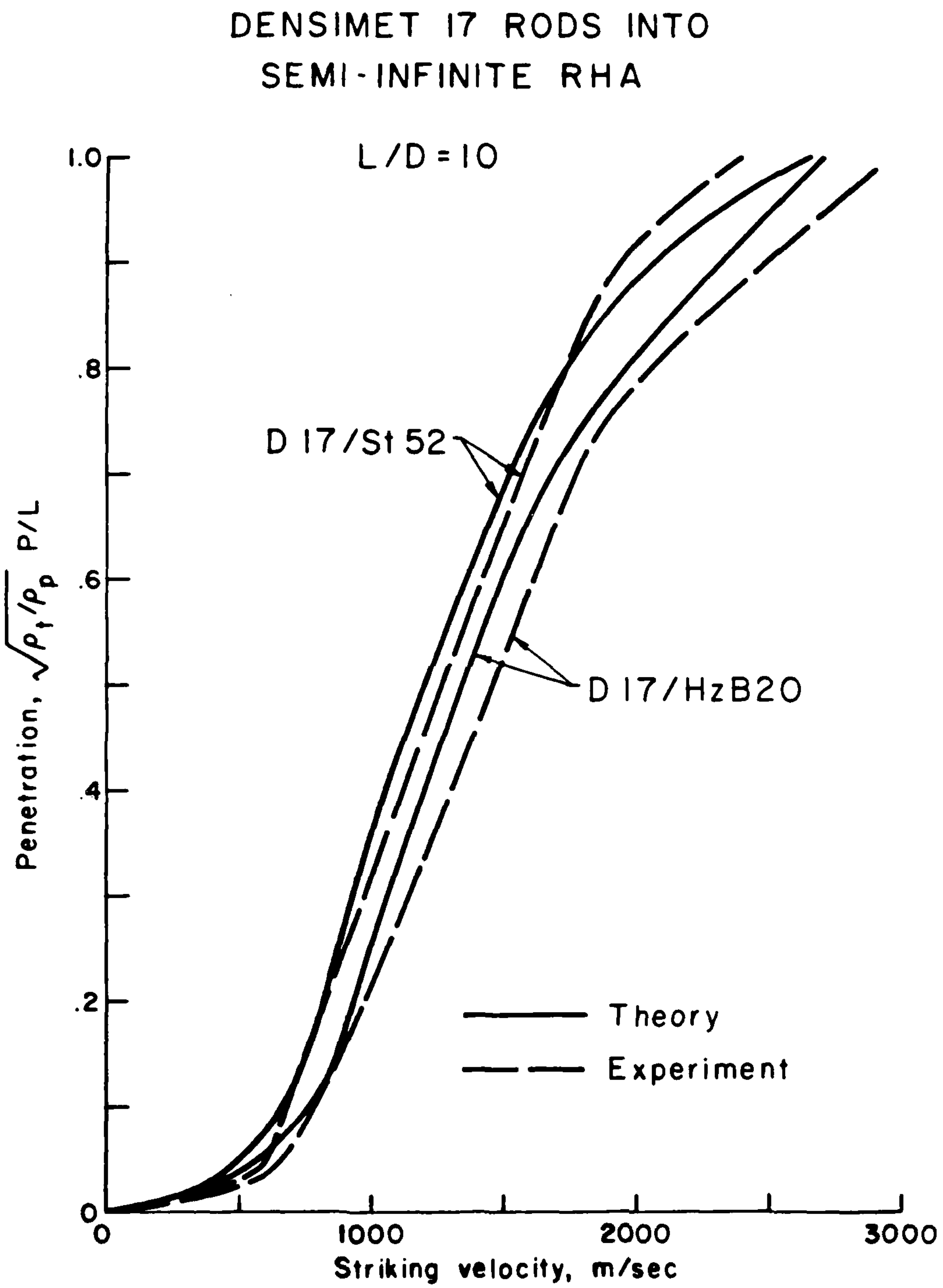
DENSIMET 17 RODS INTO
SEMI-INFINITE RHA
L/D = 10
D 17/St 52
D 17/HzB20
Theory
Experiment
Penetration, $\sqrt{\rho_t/\rho_p}$ P/L
Striking velocity, m/sec
1.0
.8
.6
.4
.2
0
0
1000
2000
3000

Figure 33

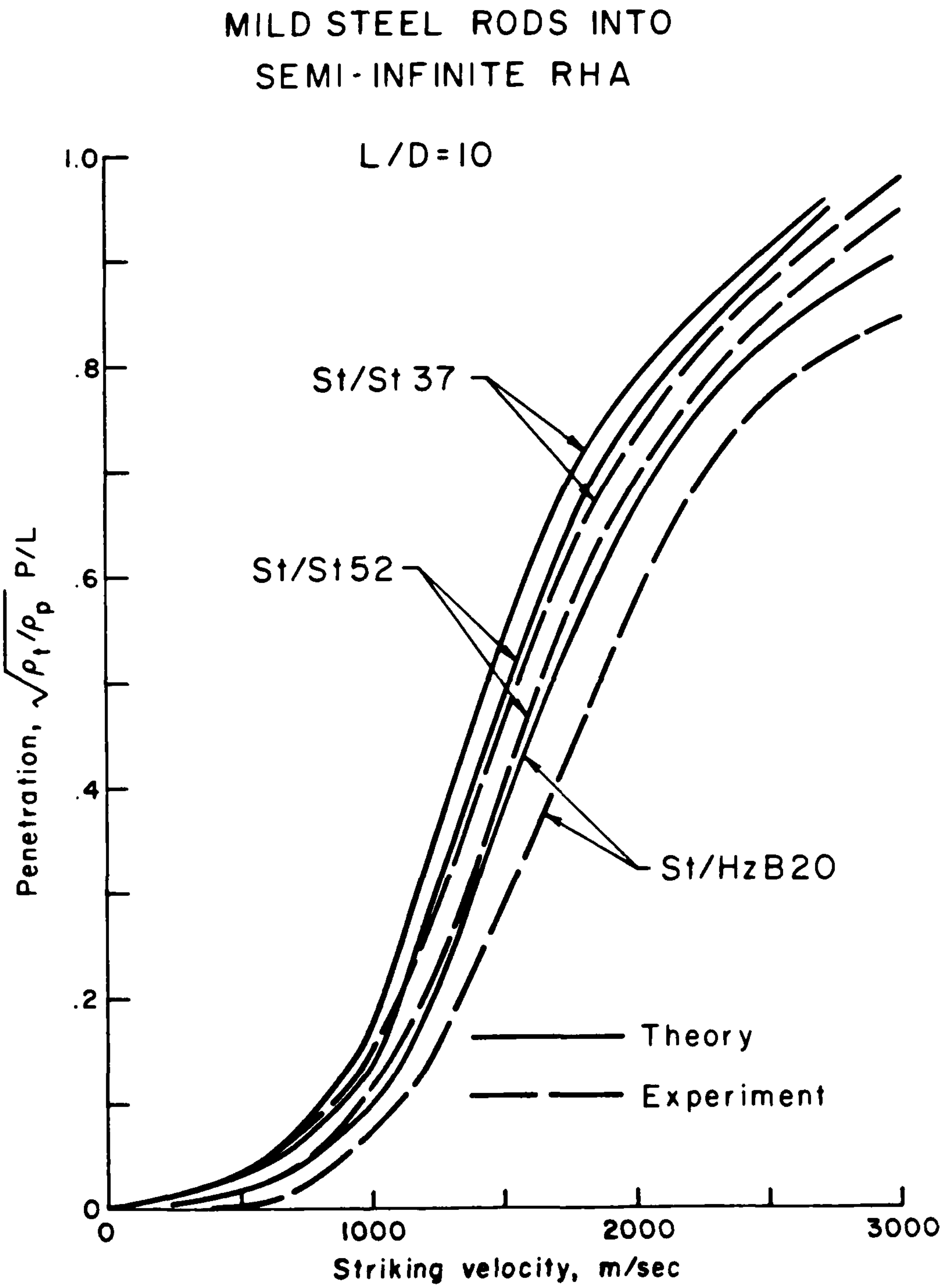
MILD STEEL RODS INTO
SEMI-INFINITE RHA
L/D=10
1.0
.8
.6
.4
.2
0
Penetration, $\sqrt{\rho_t/\rho_p}$ P/L
St/St 37
St/St52
St/HzB20
Theory
Experiment
0
1000
2000
3000
Striking velocity, m/sec

Figure 34

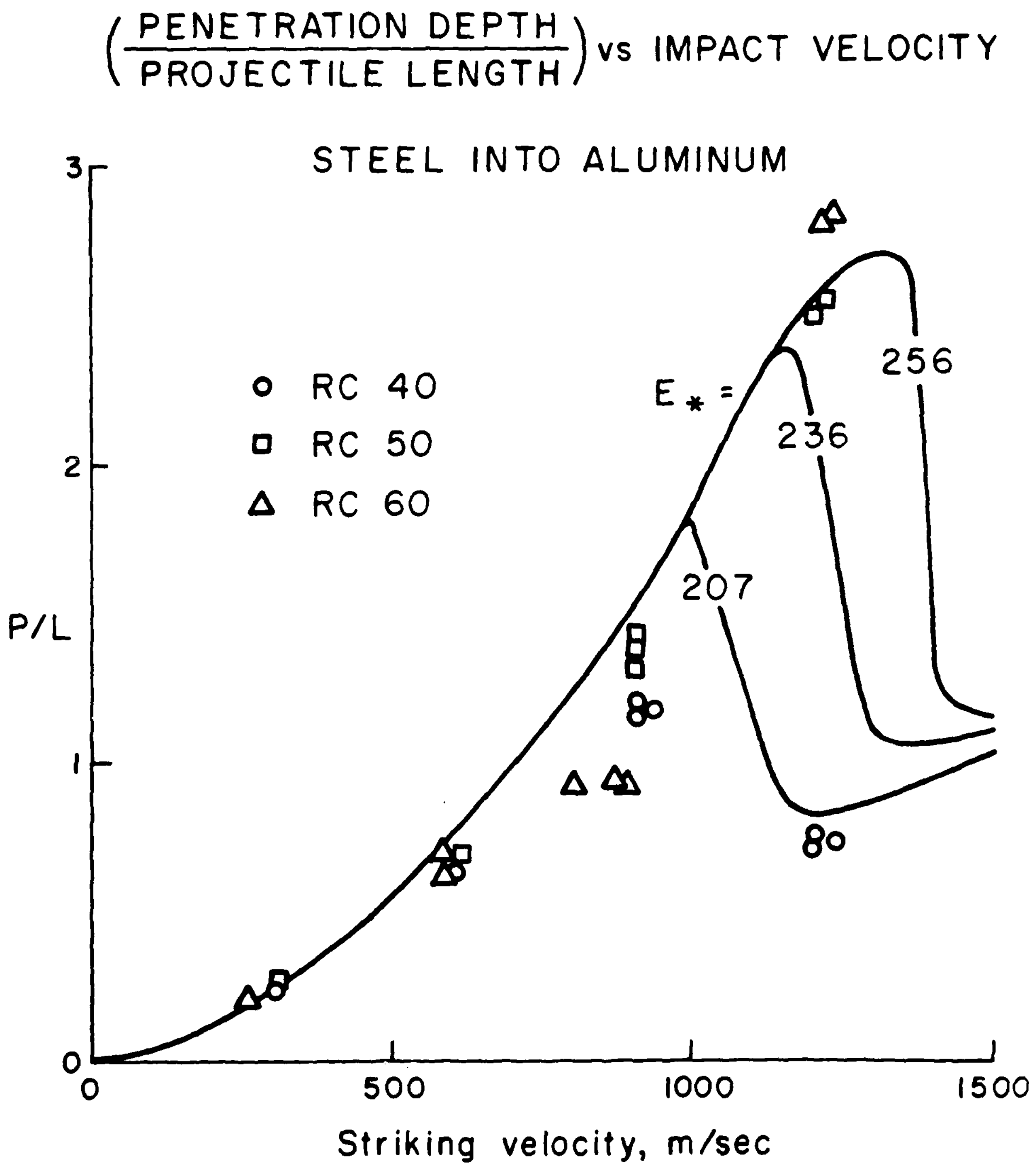

(PENETRATION DEPTH / PROJECTILE LENGTH) vs IMPACT VELOCITY
STEEL INTO ALUMINUM
RC 40
RC 50
RC 60
E* =
256
236
207
P/L
3
2
1
0
0
500
1000
1500
Striking velocity, m/sec

Figure 35

were compared to the PEN numerical code. For these data, the maximum velocity is 3000 m/sec, considerably higher than for the previous data for steel rods in Fig. 11. As Figs. 33,34 show agreement is good over the entire range of velocity for all of the materials.

Finally, the rod code was tested for the interesting case of a dense, strong rod into a low density target, in this case Bearcat steel rods into a 6061-T6 Al target.[12] The steel rod, if sufficiently strong, will not deform at low velocities and will follow the ballistic curve of a nondeforming projectile. At high enough striking velocity, the front face pressure on the rod exceeds the yield strength, and the rod begins to erode rapidly and behaves like a deforming rod. In Fig. 35, data are presented which display this transition for rods of various strengths. The theoretical curves corresponding to rods of Rockwell hardness $R_c = 40$, 50 and 60 ($E_* = 207$, 236 and 256 Btu/lb) clearly show that the stronger rod begins to deform at higher velocity. These data provide a critical test of the way the rod strength enters the code, since the transition from nondeforming to deforming rod is so sharp. Experiments such as this one provide a sensitive means for empirically determining the uniaxial adiabatic yield strength of a rod.

VII. CONCLUSIONS

The Integral Theory of Impact has been applied to the problem of modeling the behavior of long-rod penetrators. A two-cell model for the deforming rod is employed, assuming conservation of energy and momentum, and using the A.R.A.P. concept of adiabatic hardness, ρE_* , to account for material strengths. A numerical code based on these assumptions has been developed which can predict the performance of rod penetrators impacting finite thickness targets. The input parameters required to operate the code consist only of the physical dimensions of the target and penetrator, and standard handbook properties of the materials, such as density, heat capacity and Brinell hardness, which is needed to compute ρE_* .

The code predictions of ballistic limit velocity, penetration depth, residual mass and residual velocity are in good agreement (typically ±15%) with experiment over a wide range of materials and velocities. The code accurately predicts the relative improvement in performance of a rod when its strength is increased, or when the target hardness is changed, and also predicts the approximate velocity at which a rod transitions from nondeforming to deforming penetration.

The current treatment of oblique impact does not attempt to handle fracture of the rod shaft or jetting of the rod front end during impact. However, where shaft fracture is not a problem, the code predictions of ballistic limit are in good agreement with experiment.

REFERENCES

1. Donaldson, Coleman duP. and McDonough, Thomas B.: A Simple Integral Theory for Compact Cratering by High Speed Particles. DNA 3234F, Aeronautical Research Associates of Princeton, Inc., Princeton, NJ, 08540, 4 December 1973.

2. Donaldson, Coleman duP., Contiliano, Ross M., and McDonough, Thomas B.: A Study of Water Drop Displacement and Deformation in Aerodynamic Shock Layers. A.R.A.P. Report No. 265, Aeronautical Research Associates of Princeton, Inc., Janaury 1976.

3. McDonough, Thomas B. and Contiliano, Ross M.: The Sensitivity of Impact Response to the Mechanical Behavior of the Penetrator. A.R.A.P. Report No. 266, Aeronautical Research Associates of Princeton, Inc., January 1976.

4. Donaldson, Coleman duP., Contiliano, Ross M., and Swanson, Claude V.: The Qualification of Target Materials using the Integral Theory of Impact. A.R.A.P. Report No. 295, Aeronautical Research Associates of Princeton, Inc.

5. Contiliano, Ross M., and Donaldson, Coleman duP.: The Development of a Theory for the Design of Lightweight Armor. A.R.A.P. Report No. 313, Aeronautical Research Associates of Princeton, Inc., November 1977.

6. Allen, William A., and Rogers, James W.: Penetration of a Rod into a Semi-Infinite Target. J. Franklin Institute, 272, 275 (1961).

7. Hohler, V., and Stilp, A.J.: Penetration of Steel and High Density Rods in Semi-Infinite Steel Targets. 3rd International Symposium on Ballistics, March 1977, Karlsruhe.

8. Wilkins, Mark L., and Guinam, Michael W.: Impact of Cylinders on a Right Boundary. J. Appl. Phys., 44, 3, March 1973.

9. Lambert, J.P., Misey, J.J., Morfogenis, P.G., and Zukar, J.A.: Behind Armor Data for Long Rod Penetrators. B.R.L. Interim Memorandum Report No. 430, USA Ballistic Research Laboratories, Aberdeen Proving Ground, MD, September 1975.

10. Herr, Louis, and Grabanek, Chester: Ballistic Performance and Beyond Armor Data for Rods Impacting Steel Armor Plates. B.R.L. Memorandum Report No. 2575, USA Ballistic Research Laboratories, Aberdeen Proving Ground, MD, January 1976.

11. Private Communication, Konrad Frank, USA Ballistic Research Laboratories, Aberdeen Proving Ground, MD.

12. Private Communication, John H. Suckling, USA Ballistic Research Laboratories, Aberdeen Proving Ground, MD.

APPENDIX 1

LISTING OF ROD CODE

```
C      ROD WITH SHEAR AND STRENGTH
C      VERSION 2
       DOUBLE PRECISION EPST(12), ASAVE(36),ASCALE(36)
       DOUBLE PRECISION ALEN(36),VSAVE(36),ES(6),RTAR(6), THIK(12)
       DOUBLE PRECISION ESDIN
       DOUBLE PRECISION   D2,P,DP,L2,DL2,K,MA,DMA,MB,DMB,K4,K5,LOVERD,M
       DOUBLE PRECISION  MPRIM,PTARG,P2,MF,MU,B2,DB2, DMF,VO
       DOUBLE PRECISION TOVERD
       DOUBLE PRECISION EOFAIL,ESTIN,YIELD
       DOUBLE PRECISION ESTART,RHOTAR,EPSTAR,THICK, CCPEN,TMELT,RHOP
       DOUBLE PRECISION A,LENGTH
       DOUBLE PRECISION ESTFAC
       DOUBLE PRECISION VF,DVF ,DVO,DDL2,T
       DOUBLE PRECISION POVERL, PRL
       PI=3.14159
C
       ESDIN=1.0
       FLAT=0.0
       FLAT=1.0
       C1=1.0
       C2=0.0
       READ(5,888) NVELOC,NTARG,NPEN,NWRITE,NV2,NV3    ,NSCAN
 888   FORMAT(7I10)
       DO 15 I=1,NVELOC
       READ(5,12) LENGTH,A,VO
 12    FORMAT(3D10.0)
       VSAVE(I)=VO
       ALEN(I)=LENGTH
       ASAVE(I)=A
       ASCALE(I)=0.005/A
 15    CONTINUE
       DO 16 I=1,NTARG
       READ(5,11) ESTART,RHOTAR,EPSTAR,THICK
 11    FORMAT(4D10.0)
       ESTART=ESTART*1055.0*2.2
       ES(I)=ESTART
       RTAR(I)=RHOTAR
       THIK(I)=THICK
       EPST(I)=EPSTAR
 16    CONTINUE
       DO 101 J1=1,NPEN
       READ(5,10) CCPEN,TMELT,RHOP,YIELD,EOFAIL,ESTIN
 10    FORMAT(6D10.0)
       ESTIN=ESTIN*ESDIN
       YIELD=YIELD*1.0E6
       YIELD=1055.0*2.2*ESTIN*RHOP
       YIELD=0.42*YIELD
       YIELDP=YIELD
       DO 102 J5=1,NTARG
       ESTART=ES(J5)
       ESTARO=ES(J5)
       RHOTAR=RTAR(J5)
       EPSTAR=EPST(J5)
C
C      INITIALIZE PARAMETERS
       DO 103  J6=1,NVELOC
       SCALE=ASCALE(J6)
       VO=VSAVE(J6)
       A=ASAVE(J6)*SCALE
       THICK=THIK(J5)*SCALE
       LENGTH=ALEN(J6)*SCALE
       DO 96 NV1=NV2,NV3,1
```

```
      IF(NSCAN.LT. 0.5) GO TO 47
      V0=FLOAT(NV1)*100.0
 47   CONTINUE
      B2=A
      EPSFAC=0.0
      MA=0.0
      DMA=0.0
      MB=0.0
      DMB=0.0
      STR=0.0
      T=0.0
      P=0.0
      P2=0.0
      L2=LENGTH/2.0
      L2=A/6.0
      DL2=-1.0
      ALPHA1=0.4
      TEMP0=300.
      TEMP=TEMP0
      DMF=0.0
      DB2=-0.5*(DL2*B2/L2)
      M0=PI*A*A*LENGTH*RHOP
      MUMO=M0*V0
      MUMO=0.05*MUMO
      MF=2.0*L2*RHOP*A*A*PI
      MPRIM=M0-MF
      DV0=0.0
      VF=V0
      VF=VF-DL2
      ALF=6.0
      K=0.5*M0*V0*V0
      ENERG0=0.01*K
      VB=V0
      ESTARD=YIELD/RHOP
      LOVERD=LENGTH*0.5/A
      DT=1.0E-8
      DT=DT*DTIN*SQRT(RHOP/RHOTAR)
      EPFAIL=1.36
      WRITE(5,609) RHOP,LENGTH,A
 609  FORMAT(3D16.6)
      ESTCOR=ESTARD/(2.2*1055)
      WRITE(5,610) ESTCOR
 610  FORMAT(D16.6)
      VINIT=V0
      DISTH=0.0
      SPHER=0.0
      WRITE(5,991) ESTART
 991  FORMAT(D16.6,'=ESTART')
      WRITE(5,993) E0FAIL,ESTIN
 993  FORMAT( D16.6,'=E0FAIL', D16.6,'=ESTIN')
      DO 100 I=1,1000
      DO 99 J=1,100
      CD=1.0
C
C     MODIFICATION OF E0 IN HEAD
      ADEN=RHOTAR*A*(ESTART+0.5*VF*VF)
      EPS0=EPFAIL*C1+RHOP*2.0*L2*DB2*DB2*L2/ADEN
      FAC1=1.0
      FAC3=1.0
      FAC5=1.0
      FAC7=1.0
      FAC8=1.0
      FAC9=0.0
```

```
      L2=L2+DL2*DT
      DL2=DL2+DDL2*DT
C     KEEPS TRACK OF TAIL MOTION
      DISTB=DISTB+V0*DT
      V0=V0+DV0*DT
      FLAG=1.0
      IF(P.GT.P2) FLAG=0.0
      DP=VFACE*DT
C     POSITION OF FACE
      P2=P2+DP
C     POSITION OF CRATER BOTTOM
      P=P+DMAX1(DP,0.D0)*FLAG
      VF=VF+DVF*DT
      MA=MA+DMA*DT
      MB=MB+DMB*DT
      B2=B2+DB2*DT*(1.0-FAC9)
      IF(B2.GT.EPS0*A) B2=A*EPS0
      MF=2.0*PI*L2*B2*B2*RHOP
      MPRIM=M0-MF-MB
      T=T+DT
C
C     SUPERFLUOUS VARIABLES
      DTEMP=FAC5*3.0*PI*B2*B2*DL2*YIELDP/(RHOP*CCPEN)
      DTEMP=ABS(DTEMP)
      TEMP=TEMP+DTEMP*DT
C
C     CONDITION FOR HALT OF PENETRATION
      ENERGY=0.5*(M0-MF-MB)*V0*V0+0.5*MF*VF*VF
      IF(ENERGY.LT.ENERG0) GO TO 1
      MOM=(M0-MF-MB)*V0+MF*VF
      IF(MOM.LT.MOM0) GO TO 1
 99   CONTINUE
C
C     INTERMEDIATE OPTIONAL VARIABLE PRINTOUT
      IF(NWRITE.LT.0.5) GO TO 895
      WRITE(5,51)
 51   FORMAT('0')
      WRITE(5,50) P,VF,L2,B2,MF,FAC1,FAC9,FAC5,V0
      WRITE(5,50) T,VFACE,DL2,DB2,M0,DVF,K1,ENERGY ,K1
      WRITE(5,50) MA,DMA,MB,DMB,DMF, P2 ,DDL2,TEMP
 50   FORMAT(9D12.4)
      WRITE(5,55) EPS0,FYIELD
 55   FORMAT('  EPS0=',D16.6,' FYIELD=', D16.6)
 895  CONTINUE
 100  CONTINUE
C
C     FINAL VARIABLES PRINTOUT
 222  CONTINUE
      THICK=THICK/SCALE
      WRITE(5,223) THICK,EPSTAR
 223  FORMAT('0','PENETRATION OCCURS','  THICK=',E12.4,'EPSTAR=',E12.4)
 1    CONTINUE
      POVERL=P/LENGTH
      PRL=POVERL*SQRT(RHOTAR/RHOP)
      A=A/SCALE
      LENGTH=LENGTH/SCALE
      WRITE(5,998) A,V0,RHOP,LENGTH
      WRITE(5,999) ESTART,RHOTAR
 998  FORMAT('0','INITIAL: A=',D12.4,'  V0=',D12.4,'  RHOP=',D12.4,
     *'  LENGTH=',D12.4)
 999  FORMAT( 'ESTART=',D12.4,'  RHOTAR=', D12.4)
      WRITE(5,59)
 59   FORMAT('0','END OF RUN.    FINAL PARAMETERS:')
```

```
      WRITE(5,50) P,VF,L2,B2,MF,FAC1,FAC9,FAC3
      WRITE(5,50) T,VFACE,DL2,DB2,M0,DVF,R1,ENERGY
      PTARG=P+2.0*B2
      P=P/SCALE
      PTARG=PTARG/SCALE
      WRITE(5,996) VINIT,P,PTARG
996   FORMAT('0',' VINIT=',D12.4,' P=',D12.4,' PTARG=',D12.4)
      WRITE(5,601) POVERL,PRL
601   FORMAT('    POVERL=',D12.4,'    PRL=', D12.4)
      TOVERD=PTARG/(2.0*A)
      WRITE(5,843) TOVERD
843   FORMAT(' TOVERD=',D12.4)
      MR=M0-MR
      VRESID=(V0*MPRIM+VF*MF)/MR
      MR=MR/SCALE**3
      WRITE(5,224) LOVERD,VRESID,MR
224   FORMAT(' LOVERD=',D12.4,' VRESID=',D12.4,' MRESID=',D12.4)
96    CONTINUE
103   CONTINUE
102   CONTINUE
101   CONTINUE
      CALL EXIT
      END
```

APPENDIX 2

LISTING OF PEN CODE

```
      REAL L,ESTIN,EOFAIL,P,E0,MUM,MPRIM,MUMU
      REAL LENGTH
      REAL LOVERD
      REAL PBAR,PRBAR
      REAL IROT, MPRIM,M,PPERP,PPAR
      REAL MINIT, LALPH
      REAL MRBAR
      PI=3.14159
C
      READ(5,888) NVELOC,NTARG,NPEN,NPRINT
 888  FORMAT(4I10)
      READ(5,41) IV0,IV1,IDV0
  41  FORMAT(3I10)
C
C     THETA=STRIKING ANGLE, RADIANS
C     THICK=TARGET THICKNESS IN METERS.
C     ESTARS=ESTAR OF TARGET
      READ(5,42) THETA,THICK,ESTARS
 42   FORMAT(3E10.0)
C
C     NESTAR: IF ZERO,ESTART GIVEN BY   TART INPUT, IF ONE, THEN
C          ESTART GIVEN BY ESTARS.
C     NVREPL: ALLOWS SEQUENCE OF VELOCITY INCREMENTATION. IF
C          EQUAL TO ONE,THE VALUES OF IV0,IV1,AND IDV0 DETERMINE
C          THE INITIAL,FINAL, AND INCREMENT VELOCITIES.
      READ(5,887) NESTAR,NVREPL
 887  FORMAT(2I10)
      TSAVE=THICK
      THETA=THETA*PI/180.0
      DO 15 I=1,NVELOC
C
C     LENGTH=PENETRATOR LENGTH IN METERS.
C     A=PENETRATOR DIAMETER IN METERS.
C     V0=STRIKING VELOCITY.
      READ(5,12) LENGTH,A,V0
 12   FORMAT(3E10.0)
      A=A/2.0
C     ESTART=ESTAR OF TARGET IN BTU/LB.
C     RHOTAR=DENSITY OF TARGET IN KG/M3.
C     EPSTAR=NOT USED.
      READ(5,11) ESTART,RHOTAR,EPSTAR,THICK
 11   FORMAT(4E10.0)
C
      IF(NESTAR.LE.0.5) GO TO 995
      ESTART=ESTARS
 995  CONTINUE
      ESTAR0=ESTART*1055.0*2.2
      THICK=TSAVE
C
C     RHOP=PENETRATION DENSITY IN KG/M3.
C     ERREV=NOT USED.
C     ESTIN=ESTAR OF PENETRATOR MATERIAL.
      READ(5,10)  RHOP,ERREV,ESTIN
 10   FORMAT(3E10.0)
      LOVERD=LENGTH/(2.0*A)
      IF(NVREPL.LE.0.5) IV0=1
      IF(NVREPL.LE.0.5) IV1=1
      IF(NVREPL.LE.0.5) IDV0=1
      DO 999  IV=IV0,IV1,IDV0
      IF(NVREPL.LE.0.5) GO TO 996
      V0=FLOAT(IV)
 996  CONTINUE
```

```
C
C     EOFAIL=MAX WIDTH IF HYDRODYNAMIC HEAD
      EOFAIL=1.7
C     BETA=SPREADIN OF FRONT FACE
      BETA=2.0
C     GAMMA=ACCELERATION EFFECT IN FRONTFACE
      GAMMA=1.0
      EO=EOFAIL**2
      ELF=EO
      CD=0.25
      CDO=CD
      VO=1055.0*2.2*ESTIN*RHOP
      U=VO
      L=LENGTH
      ENERGO=0.5*L*PI*A*A*RHOP*U*U
      MOMO=L*A*A*PI*RHOP*U
      DT=L*0.001/VO
      P=0.0
      WRITE(6,91) EOFIX,YOFIX,BETA,GAMMA
 91   FORMAT(4E12.4)
      WRITE(6,24) ENERGO,MOMO,LENGTH,A,VO,ESTART
      WRITE(6,24) RHOTAR,EPSTAR,THICK,RHOP,EOFAIL,ESTIN
      VF=0
      MPRIM=PI*A*A*L*RHOP
      MINIT=MPRIM
      WRITE(6,24) ENERGO,MOMO,MPRIM,U,VF,P
 24   FORMAT(6E12.4)
      WRITE(6,302) EOFAIL,CD,NESTAR,NVREFL  ,BETA,GAMMA
 302  FORMAT(2E12.5,2I12,2E12.5)
      WRITE(6,300) LENGTH,A,RHOP
 300  FORMAT(' LENGTH=',E12.5,'    A=',E12.5,'  RHOP=',E12.5)
      WRITE(6,304) VO,THETA,ESTIN
 304  FORMAT('  VO=',E12.5,'  THETA=',E12.5,'  ESTIN=',E12.5)
      WRITE(6,301) RHOTAR,ESTART,THICK
 301  FORMAT(' RHOTAR=',E12.5 ,' ESTART=',E12.5,' THICK=',E12.5)
      IF(MPRIM.LE.0.5) GO TO 990
      WRITE(6,47)
 47   FORMAT('0', '     PHI          PSI         MPRIM          U            VF         '
     * ,' ',
     * DVF         P          PRBAR            VL             UL          BEND          EF          ER')
 990  CONTINUE
      NHYDRO=1
      NHYDRO=0
C     INITIALIZE
      IROT=MPRIM*L**2*(0.083)
      EO=1.0
      FL=0.0
      BEND=0.0
      DBEND=0.0
      DDBEND=0.0
      PHI=0.0
      DPHI=0.0
      DDPHI=0.0
      PPAR=0.0
      PPERP=0.0
      CHI=0.0
      UL=0.0
      DUL=0.0
      PSI=0.0
      DPSI=0.0
      ER=0.0
      EF=0.0
      VL=0.0
```

```
      SIG1=0.0
      EFAIL=0.1
      EFFAC=1.0
      CDFAC=1.0
      DO 100 J=1,1000
      DO 19 J1=1,100
C
C     COMPUTE TRIG FUNCTIONS
      SIN1=SIN(THETA)
      SIN2=SIN(THETA-PHI-PSI-4.0*BEND/L)
      COS2=COS(THETA-PHI-PSI-4.0*BEND/L)
      SIN3=SIN(PHI)
      COS3=COS(PHI)
      SIN4=SIN(PSI+PHI)
      COS4=COS(PSI+PHI)
      COS5=COS(THETA-CHI)
C
C     COMPUTE FRONT FACE EFFECTS
      TAU=THICK+A*SIN1
      SQE0=SQRT(E0)
      EF=AMIN1((P*COS5)/( A*(SIN1+SQE0*SIN2+0.0001)),1.0)
      DEL=0.0
      IF(EF.GE.0.9) DEL=0.25
      IF(EF.GE.1.0) EFFAC=0.0
      EFA=EF*COS2
      EFA=EFA*EFFAC
      EFL=EF*SIN2
      EFL=EFL*EFFAL
C
C     BACKFACE EFFECTS
C
C     COMPUTE H,DISTANCE TO BACKFACE
      PPAR=PPAR+VF*DT*COS4-VL*DT*SIN4
      PPERP=PPERP+VF*DT*SIN4+VL*DT*COS4
      P=SQRT(PPAR*PPAR+PPERP*PPERP)
      CHI=ATAN(PPERP/(PPAR+A*0.001))
      HPRIM=TAU-P*COS5
      IF(HPRIM.LE.0.0) CDFAC=0.0
      H=HPRIM
C
C     CALCULATE ER, BACKFACE RELEASE FORCE
      ER=(1.0-H/(4.0*(SQE0*EF+0.001)*A)-DEL)
      IF(ER.GE. 1.0) WRITE(6,50)
 50   FORMAT('0','PERFORATION ACHIEVED')
      IF(ER.GE. 1.0) GO TO 2
      IF(ER.LE.0.0) ER=0.0
      ERL=ER*SIN2
      ERA=ER*COS2
C
C     COMPUTE FL, LATERAL FORCE ON FACE
      VL=0.5*L*DPHI-U*SIN3+DBEND
      IF(VL.GT.0.0) SGNVL=1.0
      IF(VL.LT.0.0) SGNVL=-1.0
      IF(VL.EQ.0.0) SGNVL=0.0
      SGNVL=1.0
      FL=-( PI*A*A*E0)*(EFL-ERL)*(ESTAR0+CDD*VF*VF)
C
C     COMPUTE DDPHI
      DDPHI=0.5*FL*L/IROT
      PHI=PHI+DPHI*DT
      DPHI=DPHI+DDPHI*DT
C
C     BENDING EQUATION
```

```
      SIGBEN=PI*A*A*AMIN1(  BEND,EFAIL*A)*SIG1
      DDBEND=5.0*(FL-SIGBEN)/MPRIM
      BEND=BEND+DBEND*DT
      DBEND=DBEND+DDBEND*DT
      BEND=BEND+DL*SIN(4.0*BEND/L)
C
C     COMPUTE DUL AND DPSI
      DUL=FL/MPRIM
      UL=UL+DUL*DT
      DPSI=DUL/U
      PSI=PSI+DPSI*DT
C
C     COMPUTE VF
C
C     VF AT EARLY TIMES
      E0=ELF
      B=BETA*A
      IF((LENGTH-L)/B+1.0.LT.ELF) E0=1.0+(LENGTH-L)/B
      C1=C0*C0FAC*EF
      DVF=((C1*RHOTAR*VF*VF*E0*COS3**2-RHOP*(VF-U)**2)+RHOTAR*E0
     *    *ESTAR0*(1.0-ERA-EFA) -Y0)
      DVF=DVF*(-1.0)*GAMMA/(RHOP*A)
      VF=VF+DVF*DT
      IF(VF.LT.0.0) VF=0.0
      UFAC=1.0
      IF(VF.GE.U) GO TO 14
      GO TO 20
   14 CONTINUE
      DU=RHOTAR*E0*(COS3**2*VF**2*C1+ESTAR0*(1.0-ERA-EFA))
      DU=-DU/MPRIM
      DU=DU*PI*A*A
      U=U+DU*DT
      VF=U
      UFAC=0.0
   20 CONTINUE
      GO TO 1
   30 CONTINUE
C
C     VF DURING HYDRODYNAMIC PENETRATION
      C3=C1*COS3*COS3
      ESTAR3=ESTAR0*(1.0-ERA-EFA)
      IF(Y0/(E0*RHOTAR*C3)-ESTAR3/C3 .GE. U*U) VF=U
      IF(Y0/(E0*RHOTAR*C3)-ESTAR3/C3 .GE. U*U) GO TO 1
      FAC=U*U*RHOP/(E0*RHOTAR*C3)
      IF(Y0/(E0*RHOTAR*C3)-ESTAR3/C3+ FAC.LE.0.0) VF=0.0
      IF(Y0/(E0*RHOTAR*C3)-ESTAR3/C3+ FAC.LE.0.0)  GO TO 1
      DEL= 4.0*RHOP**2*U**2-4.0*(E0*RHOTAR*C3-RHOP)*(E0*RHOTAR*ESTAR3
     *-RHOP*U*U-Y0)
      IF( DEL.LT.0.0) WRITE(5,21)
   21 FORMAT( 'DEL LESS THAN ZERO')
      VF=-2.0*RHOP*U+SQRT(DEL)
      VF=VF*0.5/   (E0*RHOTAR*C3-RHOP)
      DVF=0.0
    1 CONTINUE
C
C     COMPUTE OTHER VARIABLES
      DU=-Y0*DT/(RHOP*L)
      U=U+DU*UFAC
      DL=(-U+VF)*DT
      IF(L.LT.0.02*LENGTH) GO TO 2
      L=L+DL
      MPRIM= L*PI*A*A*RHOP
      ENERGY=0.5*MPRIM*U*U
```

```
      MOM=L*PI*A*A*RHOP*U
      IF(MOM/MOMO .LT.0.05) GO TO 2
      IF(ENERGY/ENERGO.LE.0.01) GO TO 2
19    CONTINUE
      PBAR=P/LENGTH
      PRBAR=SQRT(RHOTAR/RHOP)*PBAR
      IF(NPRINT.LE.0.5) GO TO 991
      WRITE(6,4) PHI,PSI,MPRIM,U,VF,DVF,P,PBAR,VL,UL,BEND,EF,ER
4     FORMAT(11E10.3,2E9.2 )
991   CONTINUE
100   CONTINUE
2     CONTINUE
      LALPH=L-A
      IF( LALPH.LE. 0.0) LALPH=0.0
      VRESID=(A*VF+LALPH*U)/L
      MRBAR=MPRIM/MINIT
      TOVERD=THICK/(2.0*A)
      THETI=THETA*180.0/PI
      WRITE(6,44) THETI,THICK,TOVERD
44    FORMAT('  THETA=',E12.5,'  THICK=',E12.5,'  TOVERD=',E12.5)
      WRITE(6,45) MRBAR,VRESID
45    FORMAT('  MRBAR=',E12.5,'  VRESID=',E12.5)
      WRITE(6,7) LOVERD,VO,PRBAR
7     FORMAT('LOVERD=',E12.5,'  VO=', E12.5,'  PRBAR=',E12.5)
      WRITE(6,25)
25    FORMAT('0')
999   CONTINUE
15    CONTINUE
      CALL EXIT
      END
```